Urban Climate 64 (2025) 102716

Contents lists available at ScienceDirect

Urban Climate

journal homepage: www.elsevier.com/locate/uclim

Development and validation of the Global Urban Heat Vulnerability Index (GUHVI)

Ryan Turner [a,*], Carl Higgs [a], Chayn Sun [b], Eugen Resendiz [c,d], Ke Peng [e], Xiaoyu Cheng [e], Ruth Hunter [f], Geoff Boeing [g], Daria Pugacheva [g], Ruoyu Chen [g], Deepti Adlakha [h], Vedankur Kedar [h], Giovani Longo Rosa [i], Adewale Oyeyemi [j], Rossano Schifanella [k,l], Pau Serra del Pozo [m], Gonzalo Peraza-Mues [c,n], Joanna Valson [f], Ester Cerin [o,p], Anna Puig-Ribera [q,r], Erica Hinckson [s], Melanie Lowe [a]

[a] Centre for Urban Research, RMIT University, Melbourne, Australia
[b] School of Science, RMIT University, Melbourne, Australia
[c] Tecnologico de Monterrey, Center for the Future of Cities, Mexico City, Mexico
[d] Tecnologico de Monterrey, School of Architecture, Art and Design, Mexico City, Mexico
[e] Hunan University, Changsha, China
[f] Queens University Belfast, Belfast, UK
[g] University of Southern California, Los Angeles, USA
[h] Delft University of Technology, Delft, Netherlands
[i] Universidade Federal do Rio Grande do Sul, Porto Alegre, Brazil
[j] College of Health Solutions, Arizona State University, Phoenix, USA
[k] University of Turin, Turin, Italy
[l] ISI Foundation, Turin, Italy
[m] PhD in Geography, Barcelona, Spain
[n] Tecnologico de Monterrey, School of Government and Public Transformation, Monterrey, Mexico
[o] Australian Catholic University, Melbourne, Australia
[p] School of Public Health, The University of Hong Kong, Hong Kong, China
[q] Sports and Physical Activity Research Group, University of Vic-Central University of Catalonia (UVic-UCC), Spain
[r] Institute for Research and Innovation in Life and Health Sciences in Central Catalonia (IRIS-CC), Spain
[s] Human Potential Centre, School of Sport and Recreation, Auckland University of Technology, Auckland, New Zealand

ARTICLE INFO

Keywords:
Urban heat vulnerability
Spatial indicators
Healthy cities

ABSTRACT

Climate change increases the frequency and intensity of heatwaves, amplifying heat-related health risks in cities worldwide. Inequities in heat vulnerability arise from disparities in heat exposure, built and natural environments and population attributes that impact heat sensitivity, and socio-economic determinants of adaptive capability. A lack of internationally consistent and

Abbreviations: GUHVI, Global Urban Heat Vulnerability Index; HEI, Heat Exposure Index; HSI, Heat Sensitivity Index; ACI, Adaptive Capability Index; LST, Land Surface Temperature; LSA, Land Surface Albedo; NDVI, Normalized Difference Vegetation Index; NDBI, Normalized Difference Built-Up Index; LCZ, Local Climate Zones; POPD, Population Density; POPV, Vulnerable Population; CDR, Child Dependency Ratio; SHDI, Subnational Human Development Index; IMR, Infant Mortality Rates; iHVI, Integrated Heat Vulnerability Index; SA1, Statistical Area Level 1; EWA, Equal Weighting Approach; PCA, Principal Component Analysis; GOHSC, Global Observatory of Healthy and Sustainable Cities; GHSCI, Global Healthy & Sustainable City Indicators Software.

* Corresponding author at: Centre for Urban Research, RMIT University, Building 8, Level 11, 360 Swanston St, Melbourne, VIC 3000, Australia.
E-mail address: ryan.turner@rmit.edu.au (R. Turner).

https://doi.org/10.1016/j.uclim.2025.102716
Received 30 April 2025; Received in revised form 11 October 2025; Accepted 20 November 2025
Available online 1 December 2025

Climate resilience
Sustainable cities
Open data

accessible heat vulnerability metrics creates barriers to assessing inequities and benchmarking urban heat vulnerability between cities worldwide. To address this need, we developed the Global Urban Heat Vulnerability Index (GUHVI), applicable to cities worldwide, using open data to identify spatial inequities in heat vulnerability at the neighbourhood scale. Built from an Australia-specific heat vulnerability index, the evidence-informed framework developed for the GUHVI evaluates heat exposure, heat sensitivity and adaptive capability to holistically assess heat vulnerability. Quantitative validation for eight Australian cities demonstrated strengths of the GUHVI in spatial resolution and assessment coverage of the grid-based framework. Qualitative validation for nine diverse cities internationally was performed in collaboration with local subject matter experts with knowledge of each city context. The GUHVI addresses critical gaps in existing methods by enabling systematic and comparable measurement of heat vulnerability in diverse cities internationally. Available through our customizable open-source global indicator software, the GUHVI provides evidence on modifiable risk factors of urban heat vulnerability, to inform targeted adaptation strategies that promote climate resilience and reduce health impacts from heat.

1. Introduction

1.1. The global challenge of urban heat

Extreme heat events are among the deadliest natural hazards globally, with projected increases in frequency and intensity due to climate change (IPCC, 2022; Martín and Paneque, 2022; Guerreiro et al., 2018). These events pose particular risks to urban residents due to the 'urban heat island effect' whereby built-up areas are significantly hotter than surrounding non-urban regions. Built-up urban environments dominated by impervious surfaces such as buildings and asphalt, combined with sparse vegetation, have higher relative ambient temperatures (Bosomworth et al., 2013; Coutts et al., 2010). During extreme heat events, concentrated emissions in dense urban areas can sustain higher temperatures for longer periods, further exacerbating cooling demand and putting strain on critical infrastructure needed to cool urban environments and protect residents (Sun et al., 2024; Fan et al., 2020; Auffhammer et al., 2017; Sailor et al., 2015; Santamouris et al., 2015; Salamanca et al., 2014).

Prolonged exposure to high temperatures has severe health consequences, affecting both physical and cognitive function (Hess et al., 2023; Cao et al., 2018; Harlan et al., 2014). Between 2000 and 2019, approximately 489,000 heat-related deaths were recorded worldwide (Zhao et al., 2021), with excess neonatal mortality in low- and middle-income countries attributed to climate change-related temperature increases (Dimitrova et al., 2024). Heat-related illnesses caused by dehydration and sodium loss can lead to heat exhaustion and, in severe cases, fatal heat stroke (Eifling et al., 2024; Gauer and Meyers, 2019). Heat stress also exacerbates non-communicable diseases such as cardiovascular disease, diabetes and asthma (Xu et al., 2024; Münzel et al., 2022; Kenny et al., 2010). Additionally, extreme heat reduces the safety and productivity of outdoor labour, posing economic and social challenges (Tong et al., 2021).

Heatwaves can overwhelm health systems, particularly in low- and middle- income countries (Tong et al., 2021; Chambers, 2020). While heat affects everyone, some individuals are more vulnerable than others. The very young, elderly, chronically ill, pregnant, and those in need of care, face greater risks of heat-related illnesses and mortality (Hess et al., 2023; Sun et al., 2021; Parsons, 2009). The risk of widening inequalities within cities over time also becomes apparent due to increasing climate change impacts (Chambers, 2020).

Vulnerability to heat is influenced by the degree of heat exposure, as well as characteristics of the population and where they live (Tong et al., 2021). Urban residents' experience of heat is intrinsically linked to the built and natural environment, with land uses and the built form impacting the sensitivity of neighbourhoods to heat impacts, especially in vulnerable groups. For example, areas with green vegetation cover and shade can be significantly cooler than nearby areas without such coverage (Aram et al., 2019). The experience of urban heat and capacity to adapt is impacted by socio-economic and demographic characteristics including income, education and age in addition to physiological factors, such as underlying health conditions (Voelkel et al., 2018). Spatial heat vulnerability assessments can help identify areas where local adaptation efforts are needed most, and provide crucial data-driven insights to help guide decision-makers to reduce the impact of extreme heat, especially on those at greatest risk (Tong et al., 2021).

1.2. Heat vulnerability indexes: state of the art

Heat vulnerability assessment has been a growing area of research over the past half–century (Li et al., 2024a). It is a multi-faceted endeavour that can combine various inputs related to atmospheric conditions, physical land cover materiality, topography, built and natural environments, demographics, and anthropogenic activities (Alonso and Renard, 2020; Reid et al., 2009). Heat vulnerability studies have often focussed on a specific study area or region, which has resulted in a multitude of indexes across different parts of the world (Saguansap et al., 2024; Estoque et al., 2020; Wolf and McGregor, 2013). In 2022, the Intergovernmental Panel on Climate Change defined a conceptual framework of vulnerability, including the three key components of exposure, sensitivity, and adaptive capability (IPCC, 2022). This framework provides a basis for structuring heat vulnerability studies, however further detail is required to harmonise various complex factors. Recent comprehensive analytical heat vulnerability framework recommendations stress the

importance of carefully selecting appropriate techniques to weight inputs (Kim and Kim, 2024). The principal component analysis (PCA) and equal weighting approach (EWA) are among the most common weighting techniques in heat vulnerability assessments (Qian and Liu, 2025; Li et al., 2022). The latter follows the principle that each component has the same degree of influence on heat vulnerability and are therefore treated equally, whereas PCA applies statistical techniques to determine underlying correlation patterns within the inputs and produce data-driven weightings (Karanja and Kiage, 2021). A recent study found EWA to better align with the spatial distribution of heat-related mortality, relative to PCA (Liu et al., 2020).

Recent literature reviews have found a lack of globally applicable methods for assessing heat vulnerability (Li et al., 2024a; Cheng et al., 2021; Gonzalez-Trevizo et al., 2021), and current metrics have not been comprehensively validated for cities internationally, using both quantitative and qualitative methods (Li et al., 2022). A lack of consistency in the input criteria of existing urban heat vulnerability assessments limits the ability to comparably measure and monitor progress towards healthy, heat resilient cities worldwide. An internationally applicable and validated framework consisting of default input criteria and using globally available open data could harmonise worldwide efforts to assess urban heat vulnerability within cities. Consistent metrics could overcome barriers to obtaining much-needed information on heat vulnerability, especially in low- and middle-income countries or where official government data is lacking.

1.3. Urban heat vulnerability for global application

This study sought to address the gap in international applicability and systematic measurement of heat vulnerability and support evidence-informed planning for urban health and climate resilience in cities worldwide. We engaged a global collaborative research network to develop a Global Urban Heat Vulnerability Index (GUHVI) that is applicable to cities worldwide, and able to identify spatial inequities in heat vulnerability at the neighbourhood scale. The following research questions were addressed: 1) can a global index validly and consistently measure urban heat vulnerability in diverse cities internationally using global open datasets? 2) can a global urban heat vulnerability index identify neighbourhood-level spatial inequities within cities? 3) how do heat exposure, heat sensitivity, adaptive capability, and overall heat vulnerability vary between cities across different geographical regions, climate zones, and income groups?

The GUHVI was developed for the Global Observatory of Healthy and Sustainable Cities; a collaborative open platform for measuring and monitoring urban health and sustainability internationally (Global Healthy and Sustainable City-Indicators Collaboration, 2022). To support consistent and adaptable indicator measurement across diverse urban contexts, the Global Observatory has developed open-source software (the Global Healthy and Sustainable City Indicators (GHSCI) software) that supports indicator calculation, validation, and reporting undertaken by local city teams for cities worldwide (Higgs et al., 2024). To integrate into this platform, the GUHVI needed to be robust, scalable, and able to be used by researchers, policymakers and advocates to assess cities

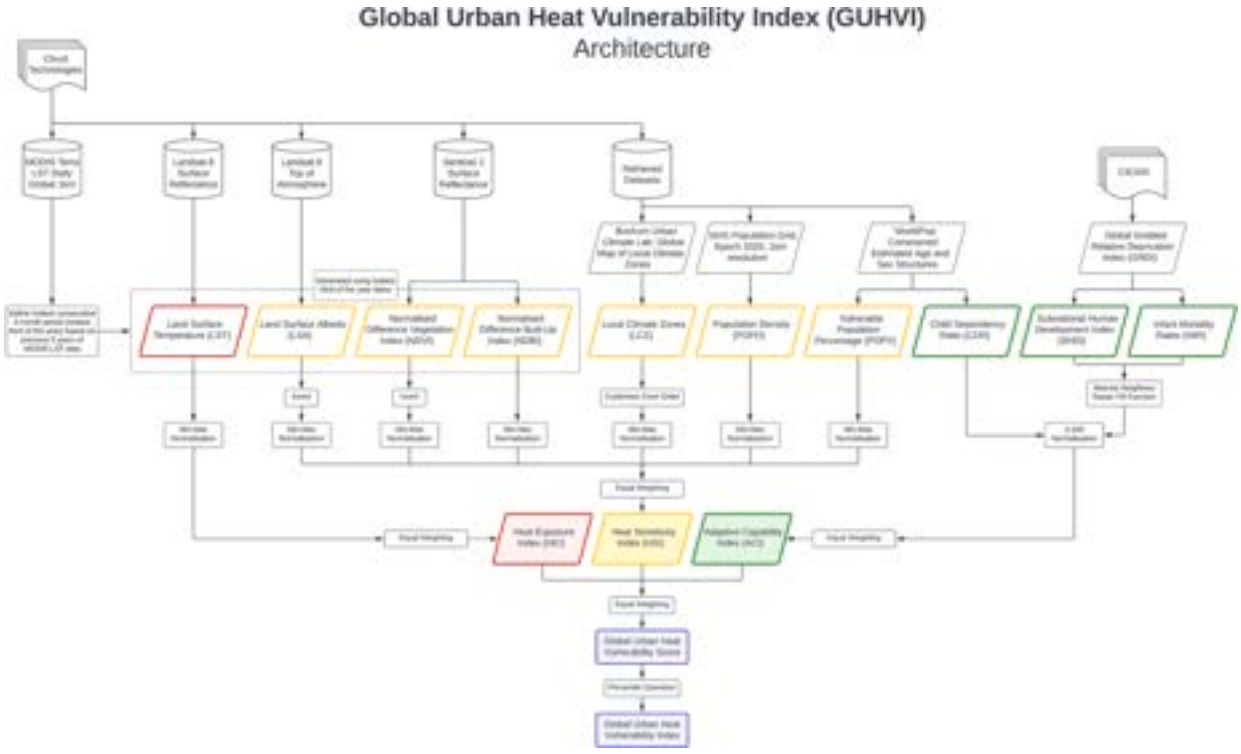

Fig. 1. GUHVI architecture diagram, indicating data sources, normalization, and equal weighting approaches.

anywhere in the world.

For this research, we adapted a heat vulnerability index developed for the Australian context (Sun et al., 2022a; Sun et al., 2019). Australia has been a focus of heat vulnerability assessment research due to the country's history of frequent extreme heat events and associated health impacts (Amoatey et al., 2025; Li et al., 2024b; Wang et al., 2023; Elizabeth Loughnan et al., 2014). Sun et al. (2019) assessed urban vegetation, urban heat island and heat vulnerability for Greater Melbourne, Victoria, subsequently developing their methods for a nationwide integrated heat vulnerability index (iHVI) toolkit (Sun et al., 2022a). The iHVI integrates multiple data sources, including remotely sensed satellite data and nationwide census data at Australia's fine scaled Statistical Area 1 (SA1) level. The iHVI generates heat exposure, sensitivity, adaptive capability, to derive an overall heat vulnerability index that provides insight into the relationships between heat, environmental, and socioeconomic factors (Sun et al., 2022a). In terms of weighting techniques, the established EWA employed by the iHVI was critically deemed as most suitable for the GUHVI as it offered a universally applicable method that would enable comparison between cities.

We developed the architecture and workflow of the GUHVI by modifying the iHVI, as it offered a robust and comprehensive assessment approach that could be adapted for global use by substituting Australian census data with global open data alternatives. Just like the iHVI, the GUHVI aligns with the conceptual framework of heat vulnerability as defined by the Intergovernmental Panel on Climate Change (IPCC, 2022), by synthesising the three components of heat exposure, heat sensitivity and adaptive capability into a composite heat vulnerability index.

2. Methods

2.1. GUHVI architecture & inputs

The GUHVI integrates ten inputs into three sub-indexes, which are then composited into a final heat vulnerability index (Fig. 1). The three sub-indexes summarised in Table 1 - Heat Exposure Index (HEI), Heat Sensitivity Index (HSI), and Adaptive Capability Index (ACI) - are well-established determinants of heat vulnerability (Kim and Kim, 2024; Li et al., 2024a; IPCC, 2022). The HEI describes the level of heat exposure using Land Surface Temperature (LST). The HSI assesses heat sensitivity as a function of Land Surface Albedo (LSA), Normalized Difference Vegetation Index (NDVI), Normalized Difference Built-Up Index (NDBI), Local Climate Zones (LCZ), Population Density (POPD) and Vulnerable Population (POPV). The final sub-index, ACI, is made up of three inputs: Child Dependency Ratio (CDR), Subnational Human Development Index (SHDI) and Infant Mortality Rates (IMR).

Table 1 lists the data sources for the ten GUHVI inputs. Inputs for the HSI differed for the GUHVI compared with those in the iHVI, due to suitability and availability of global open data. The two additional inputs of LSA and LCZ were added to more comprehensively represent land cover characteristics for global application. LSA was included as recent research suggests that increased albedo is a significant determinant of land surface temperature (Lu et al., 2023) and the strategic implementation of high-albedo materiality in urban areas can mitigate the urban heat island effect and reduce heat-related mortality (Ziaeemehr et al., 2023; Jandaghian and Akbari, 2021). Secondly, LCZ was included as an established system for describing characteristics of both grey and green land cover typologies (Stewart and Oke, 2012). A custom zone order was determined from previous studies (Rahmani and Sharifi, 2025; Zhou et al., 2020; Cai et al., 2019) that defined 'bare rock or paved' (LCZ E) as the most heat retaining, and 'water' (LCZ G) as the least heat retaining (see supplementary material for the full order). Four distinct population-related inputs were included in the HSI for the iHVI: population density, percentage aged 65+, percentage aged 4–, and percentage in need of care. In the GUHVI, population density (POPD) was retained but a single input of vulnerable persons defined as those aged 0–4 years or 65 or greater was used (POPV).

In the ACI for the iHVI, two inputs were used from Australian census data describing education and income level. In the GUHVI, education, health and living standards were captured at the global scale by the SHDI (Smits and Permanyer, 2019). CDR and IMR were also included to more holistically measure adaptive capabilities in cities internationally. Research suggests that lower instances of CDR are associated with increases in economic growth and lower poverty rates, implying a greater adaptive capability (Cruz and Ahmed, 2018). Similarly, in low- and middle-income countries, infant mortality is associated with female illiteracy and income equality with negative impacts on adaptive capacity (Schell et al., 2007).

In terms of data sources, we sourced remote sensing imagery data for LST, LSA, NDVI, NDBI, and global-scale pre-processed datasets for the remaining inputs. The 1 km resolution of the resultant GUHVI was the finest possible, based on the resolution of these datasets. For the pre-processed datasets, we used the most recently available with spatially gridded global coverage. For satellite-derived inputs, we prioritized data from the hottest period of the year (Li et al., 2024b; Reid et al., 2012).

Using data from the hottest period more accurately represents urban heat vulnerability compared with annual averages, as extreme heat events are more likely during these months. An annual average would obscure seasonal differences in temperature and fail to capture the dynamic cooling effects of vegetation, as reflected in the NDVI and LSA (Li et al., 2023; Luo et al., 2023). While many climatic studies define summer as the hottest three or four consecutive months (Shahfahad et al., 2024; Kant et al., 2020), the global scope of the GUHVI required a more nuanced approach. For instance, arid regions may experience longer hot periods, whereas high-latitude regions may have shorter ones. Closer to the equator, in tropical regions, wet and dry seasons replace the four-season cycle typical for mid-latitudes. Considering this climatic diversity, the hottest consecutive four-month period (one-third of the year) was chosen as a standard parameter for this global study.

2.2. City selection & urban centre boundaries

We included all eight Australian state and territory capital cities, and nine other cities from across six continents (Table 2).

Table 1
GUHVI data input details.

GUHVI Data Sources							
Sub-Index	Input	Name	Description	Source	Resolution	Year of data capture* or estimate**	Data Limitations
Heat Exposure Index (HEI)	**LST**	Land Surface Temperature	LST is the temperature of the Earth's surface, which gives an indication of lived experience of heat.	(Earth Resources Observation and Science (EROS) Center, 2020b)	30 m	2023–24 hottest third of the year*	These satellite-derived data sources have consistent global coverage and enable dynamic capture times, making them suitable for composite spatial indexes such as the GUHVI. However, common limitations are inconsistent repeat visit intervals and atmospheric interference, such as cloud cover.
	LSA	Land Surface Albedo	LSA measures solar reflectance, with higher values indicating greater surface reflectivity and, therefore, less surface heat retention	(Earth Resources Observation and Science (EROS) Center, 2020a)	30 m	2023–24 hottest third of the year*	
	NDVI	Normalized Difference Vegetation Index	NDVI and NDBI are spectral indices that respectively describe the land cover categories of vegetation health or greenness and impervious surfaces (e.g., concrete, asphalt)	(European Space Agency, 2021)	10 m	2023–24 hottest third of the year*	
	NDBI	Normalized Difference Built-Up Index			10 m	2023–24 hottest third of the year*	
Heat Sensitivity Index (HSI)	**LCZ**	Local Climate Zones	LCZs provide a standardized framework for urban heat island studies (Stewart and Oke, 2012)	(Demuzere et al., 2022)	100 m	2018**	Local Climate Zones are an established data source that provide an approximation of land cover typologies for global scale spatial assessments related to climate.
	POPD	Population Density	Differences in population density across urban settings are shown by POPD	(Schiavina et al., 2023)	1000 m	2025**	GHS Global Human Settlement population grid estimates are an established data source for global scale spatial assessments, and the estimate year of 2025 aligns with our analysis target year of 2023.
	POPV	Vulnerable Population Percent	POPV represents those most at risk to heat based on age, determined by the collective ratio of population aged 0–4 and 65+ years	(Tatem, 2017)	92.77 m	2020**	WorldPop provides population density, age and sex characteristics in a gridded format for global spatial assessments based on disaggregation of census data to ~100x100m grid cells through machine learning approaches. This harmonized structure allows for comparability between different cities; however, original census-data will likely offer more accurate totals and higher resolutions.
	CDR	Child Dependency Ratio	CDR is a ratio of children (aged 0–14 years) to the working population (15–64 years), indicating economic reliance		92.77 m	2020**	
Adaptive Capability Index (ACI)	**SHDI**	Subnational Human Development Index	SHDI assesses human well-being through education, health, and standard of living (Smits and Permanyer, 2019)	(Center for International Earth Science Information Network (CIESIN) Columbia University, 2022)	927.66 m	2018**	The year estimate for these two data sources may not accurately reflect the state of human development and infant mortality rates in the target year of 2023 for our GUHVI analysis. Furthermore, the coarse resolution provides less spatial detail and variance compared to the other inputs.
	IMR	Infant Mortality Rates	IMR tracks deaths in children under 1 year of age per 1000 live births in the same year; a key indicator of population health (Reidpath and Allotey, 2003)		927.66 m	2015**	

Australian cities offered the opportunity for validation against the Australian iHVI and represented a range of climate classifications, geographical areas and population estimates, from more than 5,000,000 people in Sydney and Melbourne to fewer than 150,000 in Darwin. Population density varied widely from 560 people per km^2 in Darwin to almost 2300 people per km^2 in Sydney.

The other cities were diverse in terms of geographic location, income group, population size, urban area, and climate conditions. Cities beyond Australia were selected by drawing upon the Global Observatory's existing collaborative research network (Global Healthy and Sustainable City-Indicators Collaboration, 2022). Researchers or practitioners with current or recent long-term residency in the city and expertise in city planning, healthy cities, and spatial data science were engaged as research collaborators undertaking validation for their cities.

Of the non-Australian cities, two were in lower-middle income countries (Maiduguri and Chennai), three in upper-middle income (Changsha, Porto Alegre, Mexico City), and four were in high income countries (Los Angeles, Turin, Barcelona, Belfast). Population estimates for 2025 ranged from over 485,000 in Belfast to almost 18,500,00 in Mexico City, and population density ranged from 2705 people per km^2 in Los Angeles to 12,397 people per km^2 in Chennai. The hottest third of the year date range varied across the included

Table 2
City profiles demonstrating diverse range of climate zones, income group and population statistics. Hottest third of the year calculated for each city is listed in the final column.

City Profiles							
Region and Country	City	Köppen-Geiger climate classification*	Income group**	Urban centre boundary area (km^2)	2025 population projection***	Population density (per km^2)	Hottest third of the year date range
Africa							
Nigeria	Maiduguri	BSh	Lower-middle	233	1,295,169	5559	23–03-01 to 23–07-01
Asia							
India	Chennai	Aw	Lower-middle	909	11,268,605	12,397	23–03-01 to 23–07-01
China	Changsha	Cfa	Upper-middle	420	3,236,226	7705	23–06-01 to 23–10-01
America, South							
Brazil	Porto Alegre	Cfa	Upper-middle	242	1,417,495	5857	23–11-01 to 24–03-01
America, North							
Mexico	Mexico City	Cwb, BSk	Upper-middle	2312	18,322,420	7925	23–03-01 to 23–07-01
USA	Los Angeles	Csa, BSh, BSk, Csb	High	5534	14,967,143	2705	23–06-01 to 23–10-01
Europe							
Italy	Turin	Cfa	High	207	1,245,485	6017	23–05-01 to 23–09-01
Spain	Barcelona	Csa, BSk, Cfa	High	548	4,602,806	8399	23–05-01 to 23–09-01
UK	Belfast	Cfb	High	160	485,512	3034	23–05-01 to 23–09-01
Oceania							
Australia	Adelaide	BSk, Csb, Csa	High	854	1,279,317	1498	23–11-01 to 24–03-01
	Brisbane	Cfa	High	2027	2,407,177	1188	23–11-01 to 24–03-01
	Canberra	Cfb	High	393	409,473	1042	23–11-01 to 24–03-01
	Darwin	Aw	High	240	134,475	560	23–09-01 to 24–01-01
	Hobart	Cfb, BSk	High	237	190,195	803	23–12-01 to 24–04-01
	Melbourne	Cfb, BSk	High	2881	5,185,199	1800	23–12-01 to 24–04-01
	Perth	Csa	High	1720	2,117,428	1231	23–11-01 to 24–03-01
	Sydney	Cfa	High	2194	5,037,214	2296	23–11-01 to 24–03-01

* Köppen-Geiger climate classifications: Aw: tropical, savannah; BSh: arid, steppe, hot; BSk: arid, steppe, cold; Csa: temperate, dry summer, hot summer; Csb: temperate, dry summer, warm summer; Cwb: temperate, dry winter, warm summer; Cfa: temperate, no dry season, hot summer; Cfb: temperate, no dry season, warm summer; Dfa: cold, no dry season, hot summer; Dfb: cold, no dry season, warm summer; Dfc: cold, no dry season, cold summer (Beck et al., 2018).

** Income group by country (The World Bank, 2024).

*** GHS Global Human Settlement population grid estimate for 2025 (Schiavina et al., 2023).

cities, reflecting the diversity of climatic zones.

The term 'urban centre' is used to describe the boundaries defined for each city in this study. Boundaries for the Australian cities were sourced from the Australian Bureau of Statistics' 'Urban Centres and Localities' (Australian Bureau of Statistics, 2022) to enable comparative analysis and validation against the Australian iHVI. To ensure consistent delineation of urban centres across the remaining cities, study region boundaries were sourced from the GHS-UCDB Global Human Settlement Urban Centre Database 2015 (Florczyk et al., 2019). In this dataset, urban centres are defined by a combination of specific cut-off values for resident population and built-up surface share, representing spatially continuous urbanized areas. The GHS-UCDB boundaries were used for the cities of Changsha, Mexico City, and Turin whereas the coastal cities of Chennai, Los Angeles, Barcelona, and Belfast had their GHS-UCDB boundaries clipped to the coastline to exclude the impact of adjacent ocean on land area calculations (see supplementary material). After feedback from collaborators in Maiduguri and Porto Alegre, it was determined that intersecting the local municipality boundary with the GHS-UCDB boundary provided a more accurate representation.

2.3. Sub-index calculation

Firstly, we selected 2023 as the target year for the satellite data derived inputs for each city (LST, LSA, NDVI, NDBI). This methodology of selecting one target year not only aligns with the GHSCI software analysis workflow but also preserves extreme values within a single year standardized baseline, enabling identification of areas within cities that have relatively higher heat vulnerability and direct comparability between cities. Next, the urban centre boundary was buffered by 1 km, and an empty 1 km square grid was created based on this buffered geometry. For each cell in this grid, the overlap percentage with OpenStreetMap (OpenStreetMap Contributors, 2024) coastline geometries was calculated (see supplementary material). This ensured that pixels overlapping ocean were weighted less than pixels entirely representing land cover in coastal cities.

Next, we programmatically identified the hottest time of year for each city from MODIS Terra satellite data which provides daily day-time LST readings globally at 1 km resolution (Wan et al., 2021). Satellite-derived LST data exhibits seasonal trends, and can be used to define the hottest time of the year (Shahfahad et al., 2024). The five-year average (2018–2022) LST for each month and for each unique consecutive four-month period was calculated to identify the hottest third of the year ('hottest period'). The corresponding months in 2023 were used as the capture dates for the satellite-derived LST, LSA, NDVI and NDBI data inputs.

LST was calculated from Landsat 8 Surface Reflectance imagery and a conversion algorithm was used to generate LSA from Landsat 8 Top of Atmosphere Reflectance (Liang, 2001). Sentinel 2 Surface Reflectance imagery was used to calculate NDVI and NDBI. Next, the LCZ data package was imported and a custom zone order from least to most heat retaining was applied (see section 2.1). POPD was derived from the GHSL population grid. POPV and CDR were calculated by their respective age group ratios using band arithmetic. Finally, the SHDI and IMR data sources were imported, and a raster nearest neighbour fill operation was performed to fill blank pixels.

All ten inputs were clipped to the buffered urban centre boundary. As high vegetation and albedo values in the NDVI and LSA inputs imply low heat vulnerability, these two were inverted to align with the remaining eight inputs, whereby high values imply high heat vulnerability. The 1 km grid was overlaid over each input layer, and then for each 1 km pixel, a spatial minimum and maximum operation was performed at the input layers' native resolution. These values were then associated with the 1 km pixel that they fall within. This aggregation process ensured that the detailed insights offered by the relatively high-resolution of the native data were captured before aggregation to the coarser uniform 1 km resolution. Next, another band containing the coastline overlap percentage value was added and min-max normalization was applied, weighting boundary pixels that overlap ocean less than those fully representing land cover. As the SHDI and IMR were already normalized to a scale of 0–100, the CDR input was also normalized in this way to ensure consistency within the ACI sub-index. The resultant normalized value was added as an additional band to each raster.

The three HEI, HSI, and ACI sub-indexes were generated by equally weighting the normalized value band of each input. These were equally weighted to generate the GUHVI score within a range from 0 to 100. Next, the 20th, 40th, 60th, and 80th percentiles of this raster were determined, and a corresponding score of 1–5 was applied to each pixel, resulting in the final GUHVI raster, where class 5 represented areas above the 80th percentile and therefore the most vulnerable to heat. For each of the ten input rasters, the three sub-index rasters, and resultant GUHVI raster, normalized mean results were determined for comparison purposes. Additionally, population percentage statistics per heat vulnerability class were calculated to illustrate the relationship between the distribution of heat vulnerability and population density for each city. Finally, we created figures for visual comparisons of differences in the distribution of heat vulnerability between and within cities.

2.4. Australian cities validation

For validation of the eight Australian cities, each city's GUHVI output was quantitatively compared to its iHVI output (Sun et al., 2022a; Sun et al., 2019). Firstly, GUHVI was generated for each city as detailed in section 2.3. For consistency, the hottest period generated for the GUHVI was also used for the satellite-derived inputs of the iHVI. The remaining iHVI inputs were sourced from Australian socio-economic data integrated in the iHVI desktop application (Sun et al., 2022a) for the most recently available census year of 2021. These census data were available for Statistical Areas Level 1 (SA1), statistical geographic areas having an average population of approximately 400 people (Australian Bureau of Statistics, 2021). Some SA1 polygons are non-residential (e.g., airports, industrial areas, education campuses, parks or playgrounds, vegetation corridors, golf courses or cemeteries) and lack corresponding socio-economic data, such as population density and income. iHVI outputs were only generated for SA1 polygons that had valid data for all inputs.

The GUHVI and iHVI were compared in QGIS (QGIS Development Team, 2024). The GUHVI raster was resampled from 1 km to 10

m resolution. Then, the iHVI polygons were converted to rasters at 10 m resolution and the output extent was copied from the resampled GUVHI raster. In this way, the rasterized iHVI had the exact same grid geometry as the GUHVI, allowing for direct comparison. Rasterising the iHVI polygons at a spatial resolution of 10 m rather than the GUHVI raster's native resolution of 1 km reduced information loss (Bai et al., 2011; Congalton, 1997) in the level of detail of the SA1 boundaries and still allowed for direct comparability as the two spatial resolutions were equally divisible.

Using the raster calculator, areas of heat vulnerability class agreement, plus or minus one class difference, and greater than one class difference were generated and expressed as an area percentage of the GUHVI and iHVI comparison overlap area. The percent of the urban centre boundary area with no iHVI output was also generated. Pearson's correlation coefficient was generated to describe linear correlation where both the GUHVI and iHVI had data. Normalized mean differences were also generated for the iHVI outputs and are available in supplementary material. Lastly, visualisations were created which compared spatial distributions of heat vulnerability class definitions between the two indexes.

2.5. International cities validation

For validation of the GUHVI outputs for cities beyond Australia, collaborators provided qualitative feedback on the initial results between 11th June and 5th July 2024, based on local knowledge of their city. For each city, GUHVI data outputs and a QGIS project file were sent to collaborators along with an instructional video providing an overview of how to validate the index using the QGIS project (see supplementary material).

A live Google Sheets spreadsheet was used to capture structured feedback for each city from collaborators and comments were

Table 3
GUHVI results of mean heat exposure, heat sensitivity, adaptive capability, overall heat vulnerability and population percent per heat vulnerability class for each Australian and international city.

Global Urban Heat Vulnerability Index (GUHVI) - Results									
City	Normalized Mean				% of population per heat vulnerability class				
	Heat Exposure Index (HEI)	Heat Sensitivity Index (HSI)	Adaptive Capability Index (ACI)*	Overall Heat Vulnerability (GUHVI)**	1	2	3	4	5
International Cities									
Maiduguri	68.6	51.7	88.6	69.6	8.6	14.3	20.2	9.1	47.8
Chennai	60.3	45.7	30.7	45.6	7.2	10.4	16.7	23.8	41.9
Changsha	60.5	51.6	19.6	43.9	14.9	10.7	16.9	17.4	40.1
Porto Alegre	49.3	50.0	23.0	40.8	4.8	9.5	20.0	29.1	36.6
Mexico City	59.7	55.1	24.0	46.2	7.1	13.1	17.4	24.4	38.1
Los Angeles	70.5	52.2	10.5	44.4	9.3	13.5	20.8	21.8	34.7
Turin	41.5	53.7	9.8	35.0	6.1	11.6	14.7	16.3	51.3
Barcelona	62.3	51.5	9.2	41.0	7.2	9.0	14.9	27.1	41.8
Belfast	43.2	46.5	14.3	34.7	9.7	19.2	13.6	25.5	32.1
Summary									
Mean	*57.3*	*50.9*	*25.5*	*44.6*	*8.3*	*12.4*	*17.2*	*21.6*	*40.5*
SD	*10.4*	*3.1*	*24.8*	*10.3*	*2.9*	*3.1*	*2.6*	*6.3*	*6.1*
Min	*41.5*	*45.7*	*9.2*	*34.7*	*4.8*	*9.0*	*13.6*	*9.1*	*32.1*
Max	*70.5*	*55.1*	*88.6*	*69.6*	*14.9*	*19.2*	*20.8*	*29.1*	*51.3*
Australian Cities									
Adelaide	66.2	48.7	8.9	41.3	7.3	12.7	23.5	23.0	33.5
Brisbane	56.6	40.9	11.0	36.1	4.7	8.4	14.1	26.1	46.6
Canberra	58.1	40.4	7.2	35.2	7.6	11.9	18.9	24.5	37.1
Darwin	58.4	37.9	9.3	35.2	12.7	7.9	21.1	28.7	29.6
Hobart	46.2	34.7	9.8	30.2	16.0	13.6	16.4	22.4	31.6
Melbourne	56.0	40.1	9.2	35.1	6.2	11.6	20.1	27.9	34.2
Perth	60.5	44.0	9.3	37.9	8.7	13.3	17.0	26.5	34.6
Sydney	49.5	39.6	9.8	33.0	6.6	9.4	17.5	28.6	37.9
Summary									
Mean	*56.4*	*40.8*	*9.3*	*35.5*	*8.7*	*11.1*	*18.6*	*26.0*	*35.6*
SD	*5.8*	*4.1*	*1.1*	*3.2*	*3.7*	*2.2*	*3.0*	*2.5*	*5.2*
Min	*46.2*	*34.7*	*7.2*	*30.2*	*4.7*	*7.9*	*14.1*	*22.4*	*29.6*
Max	*66.2*	*48.7*	*11.0*	*41.3*	*16.0*	*13.6*	*23.5*	*28.7*	*46.6*
Overall Summary									
Mean	*56.9*	*46.1*	*17.9*	*40.3*	*8.5*	*11.8*	*17.9*	*23.7*	*38.2*
SD	*8.4*	*6.3*	*19.4*	*8.9*	*3.2*	*2.7*	*2.8*	*5.2*	*6.1*
Min	*41.5*	*34.7*	*7.2*	*30.2*	*4.7*	*7.9*	*13.6*	*9.1*	*29.6*
Max	*70.5*	*55.1*	*88.6*	*69.6*	*16.0*	*19.2*	*23.5*	*29.1*	*51.3*

* The lower the value, the greater the adaptive capability.
** Each index is equally weighted to determine the resultant heat vulnerability, whereby $GUHVI = (HEI + HSI + ACI)/3$.

provided on the accuracy of our methodology to identify spatial inequities in heat exposure, heat sensitivity, adaptive capability, and the overall heat vulnerability index. Please see supplementary material for the full spreadsheet. Where validation queries were raised by collaborators, we investigated the reasons behind inaccuracies in our GUHVI generation. Based on feedback and comments received during this validation exercise, changes were made to the methodology. These changes involved use of the hottest period of the year for the satellite-derived indices rather than an annual average (see section 2.1) and updating the urban centre boundary overlap methodology (see section 2.3) to only reduce weighting of coastal pixels overlapping ocean, rather than any pixel overlapping the urban centre boundary. A second round of validation was performed between 22nd January and 7th February 2025, to gather feedback about the accuracy of the hottest third of the year for each city and how using this date range for the satellite-derived inputs affected the overall GUHVI.

3. Results

3.1. GUHVI results

Table 3 summarises the results for each city. The normalized mean values of heat exposure, heat sensitivity, adaptive capability, and overall heat vulnerability are expressed on a scale of 0 to 100. As the HEI and HSI sub-indices approach 100, the greater the heat vulnerability. The adaptive capability index is reverse-scaled to match this behaviour, with higher values indicating lower adaptive capability and thus greater heat vulnerability.

Mean heat vulnerability among Australian cities ranged from 30.2 in Hobart to 41.3 in Adelaide; Hobart had the lowest mean HEI and HSI, and Adelaide had the greatest. Some cities, such as Hobart and Darwin, had their population more evenly distributed across the 5 classes. Brisbane had the highest population percentage in areas most vulnerable to heat, but all Australian cities analysed had the highest population percentage in class 5 areas, relative to the other classes.

For the international cities, ACI had the greatest variability of the indexes (standard deviation, SD 24.8). The two lower-middle income country cities of Chennai (tropical, savannah) and Maiduguri (arid, steppe, hot) had the least adaptive capability, with an ACI of 30.7 and 88.6, respectively. The upper-middle incomes country cities of Changsha, Porto Alegre, and Mexico City all had mean ACI results of less than 25, while high-income countries were all less than 15.

However, stronger adaptive capability does not imply lower overall vulnerability. The high-income city of Los Angeles had a high overall heat vulnerability which suggests that, on average, it is more vulnerable than the upper-middle income country cities of Changsha and Porto Alegre. This could be due to Los Angeles having the greatest mean level of heat exposure across all cities studied. Furthermore, the HSI result for Chennai suggests that, on average, it is the least sensitive to heat in comparison to the other international cities.

Of the international cities, Belfast and Turin had the lowest mean heat vulnerability at 34.7 and 35.0 respectively. However, over

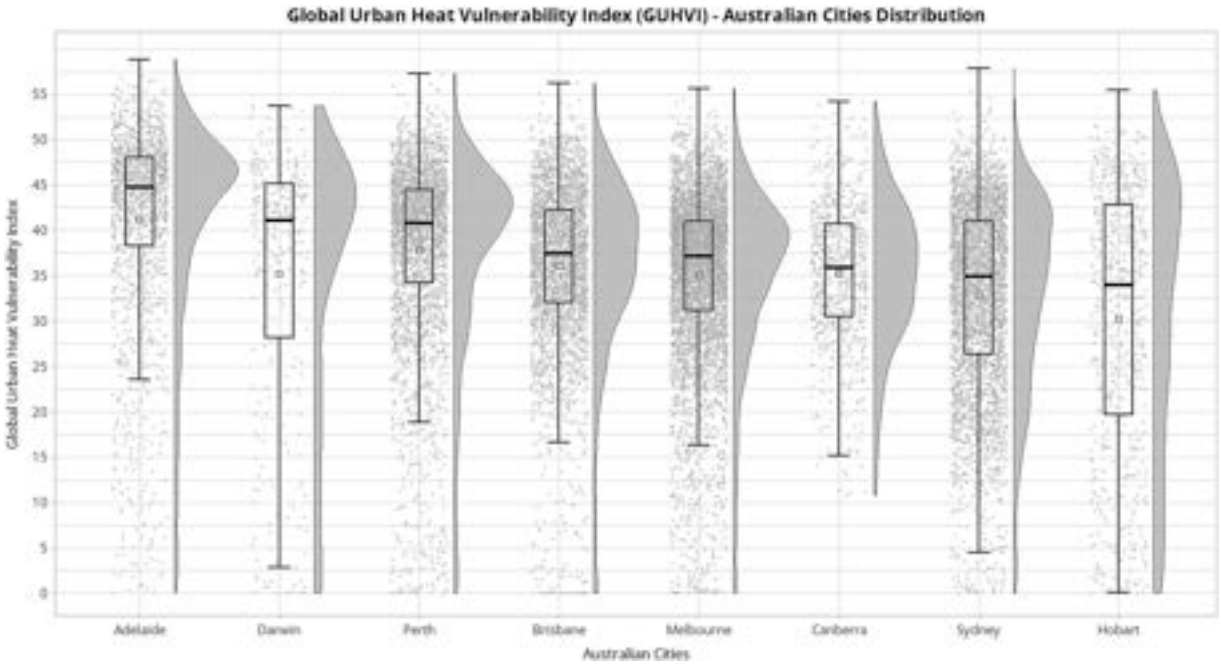

Fig. 2. Combined box, half violin, and strip plot for Australian cities, ordered from left to right in descending order of median. The strip plots show all the raw data points (jittered horizontally), the half violin plots show the distribution, and the box plots show the extrema (whisker tails), interquartile range (box boundaries), median (horizontal line), and mean (square outline).

51 % of Turin's population were found to reside in areas that are most heat vulnerable (class 5) in comparison to just over 32 % in Belfast. Indeed, similar to the Australian cities, for all international cities, the highest heat vulnerability class contained the highest percentage of the population while there were much lower percentages of the population in the least vulnerable classes.

For the Australian cities, within city differences in heat vulnerability are further contextualised in Fig. 2. All half violin plots are negatively skewed, with especially long-tailed distributions in coastal cities (all except Canberra) that have a boundary overlap with ocean. As indicated by the interquartile range, Hobart has the widest distribution of heat vulnerability.

Fig. 3 shows a wider range in heat vulnerability for the international cities. Maiduguri's maximum instance of heat vulnerability was greater than 85, compared to Turin's maximum at just below 55. Porto Alegre has the largest interquartile range, suggesting a wide distribution of heat vulnerability. Belfast has the lowest median and mean of all international cities, but has the largest range, indicating greater levels of inequity in heat vulnerability. The density of the strip plots reflect the relative size of each city in terms of land area. With Los Angeles as the largest, it has the most densely illustrated strip plot, and vice versa for Belfast.

Figs. 4 and 5 depict the spatial distribution of heat vulnerability for the eight Australian cities, and the nine international cities, respectively. The general spatial pattern of lower vulnerability at the urban periphery and greater vulnerability in the middle and inner areas can be observed for most cities, especially in Turin. However, clusters of high vulnerability on the edges can also be seen in many cities, such as Belfast, Changsha, Porto Alegre and Melbourne.

3.2. Australian cities validation results

Table 4 shows the comparison results between the GUHVI and iHVI outputs for the Australian cities, expressed as a percentage of the comparison overlap area. The percentage of the urban area for which there was class agreement or near-agreement between the indexes (plus or minus one class difference) could be viewed as an indication of areas with reasonable agreement. In this regard, there was over 75 % agreement/near-agreement between the two indexes for five of the eight cities, with results varying from 63.98 % in Canberra to 86.70 % in Melbourne. In terms of exact class agreement between the two indexes, Canberra had the lowest proportion of the urban area with agreement, at 25.60 %, and Melbourne had the highest at 45.11 %. Canberra had the lowest proportion of the urban area that was plus or minus one class difference compared to the iHVI, at 38.38 %, while Hobart had the greatest at 44.92 %. The proportion of the urban area that was greater than one heat vulnerability class difference to the iHVI varied from 36.01 % in Canberra to 13.29 % in Melbourne. Hobart had the lowest percentage of absent iHVI output, at just under 5 %, with the greatest being Darwin at just over 37 % of its total urban centre boundary area. Pearson's correlation coefficient ranges from −1 to 1, whereby 1 indicates a perfect positive linear correlation. A range of positive correlation coefficients are seen between the GUHVI and iHVI, whereby Melbourne and Sydney show the strongest positive linear association at over 0.7 each, ranging down to Darwin at 0.28. For more detailed

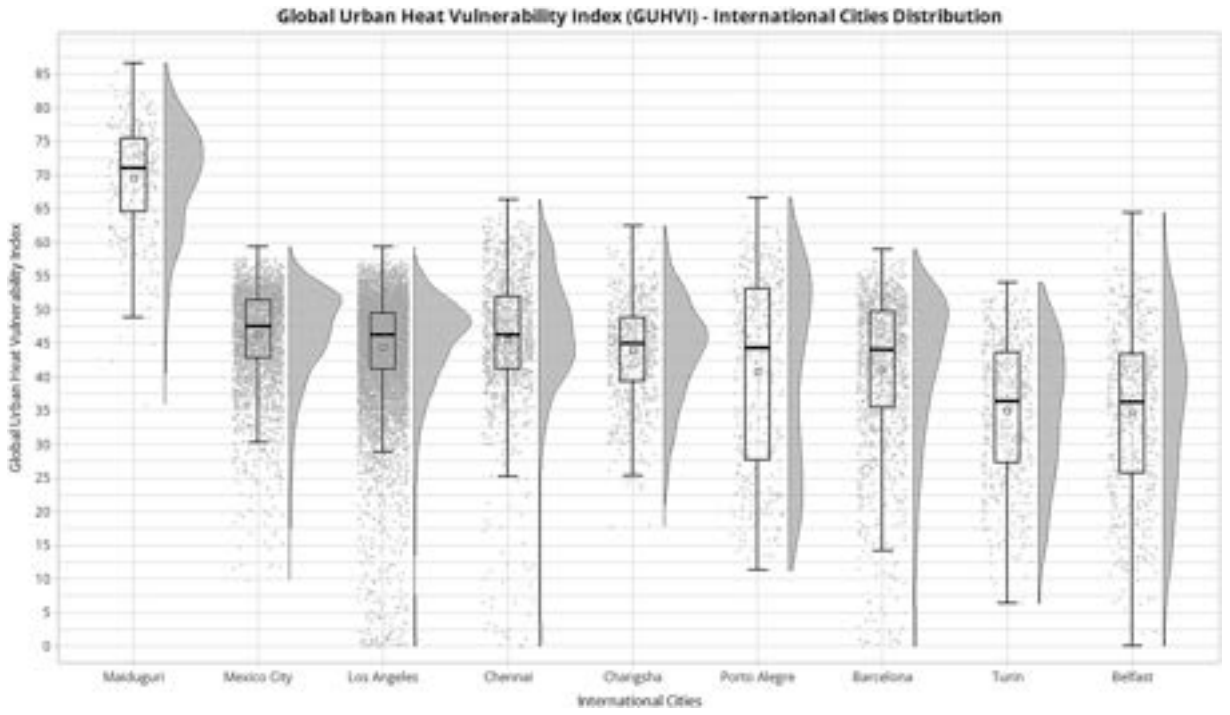

Fig. 3. Combined box, half violin, and strip plot for each international city, ordered from left to right in descending order of median. The strip plots show all the raw data points (jittered horizontally), the half violin plots show the distribution, and the box plots show the extrema (whisker tails), interquartile range (box boundaries), median (horizontal line), and mean (square outline).

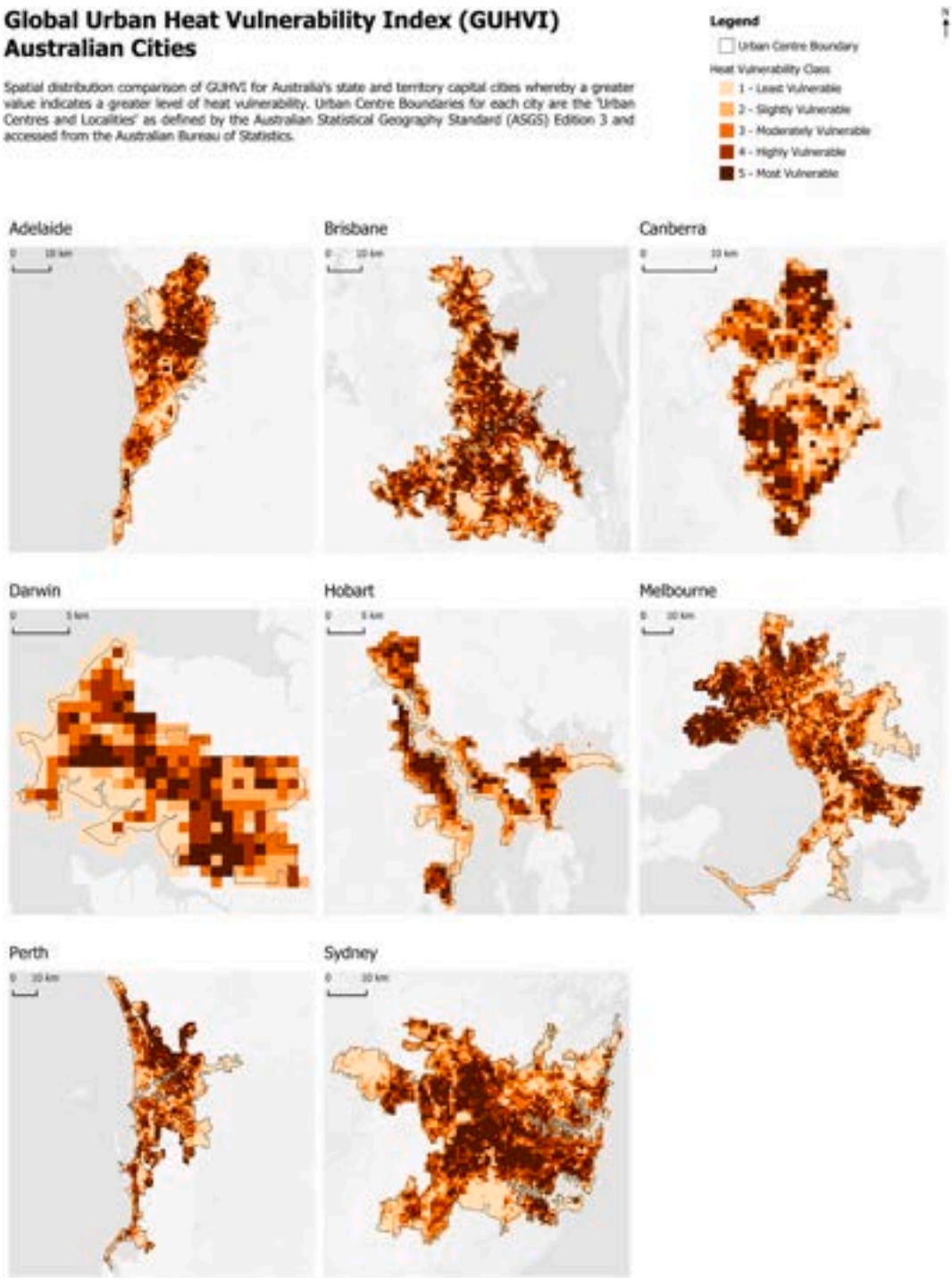

Fig. 4. GUHVI for Australian cities visualised on a 1-5 class scale of vulnerability.

comparisons between the sub-indexes, iHVI normalized mean results were also calculated for Australian cities and are available in supplementary material.

Fig. 6 is a visual summary of this comparison between the GUHVI and iHVI, showing the areas of agreement and disagreement. The supplementary material includes a side-by-side visual comparison of the GUHVI and iHVI.

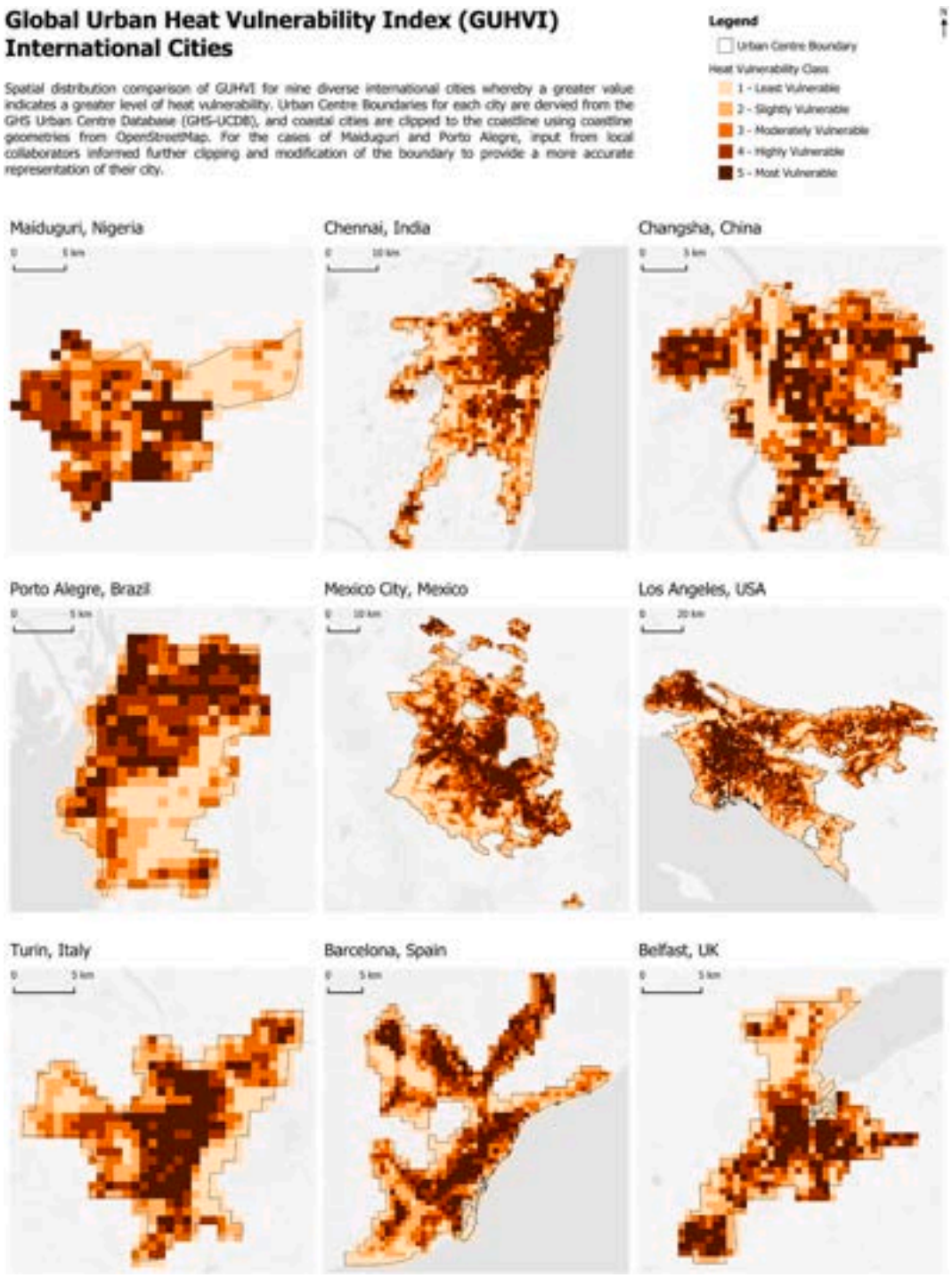

Fig. 5. GUHVI for international cities visualised on a 1-5 class scale of vulnerability.

3.3. International city validation results

Local collaborators reached consensus that the results were reasonable and accurate based on local knowledge of each city. Validators for eight of the nine cities agreed that the GUHVI was able to sufficiently identify spatial inequities in heat vulnerability. Validators for Mexico City noted uncertainty in relation to the ACI results due to "little variance across the study area" compared to the HEI and HSI. This point was corroborated by other city respondents, who indicated that there were minimal within-city differences in

Table 4
Comparison between GUHVI and iHVI heat vulnerability class agreement and disagreement.

GUHVI and iHVI Comparison Results						
Australian Cities	% of GUHVI and iHVI comparison overlap area			Agreement or ± 1 Class Difference %	% of urban centre boundary area with no iHVI data	Pearson's correlation coefficient
	>1 Class Difference	±1 Class Difference	Agreement			
Adelaide	20.26	43.86	35.88	79.74	21.87	0.52
Brisbane	32.51	40.66	26.82	67.48	17.91	0.58
Canberra	36.01	38.38	25.60	63.98	30.28	0.44
Darwin	30.52	40.80	28.68	69.48	37.06	0.28
Hobart	24.29	44.92	30.77	75.69	4.99	0.51
Melbourne	13.29	41.59	45.11	86.70	12.01	0.71
Perth	16.03	42.31	41.66	83.97	12.58	0.65
Sydney	17.14	44.72	38.14	82.86	19.16	0.71

the ACI. Validators for all cities except Los Angeles agreed that the HEI sub-index was able to identify spatial inequities in heat exposure. Respondents from Los Angeles noted that the difference in final normalization value between boundary pixels and non-boundary pixels was mild considering the actual difference in land surface temperature. For the HSI sub-index, all cities agreed upon its ability to identify spatial inequities in heat sensitivity.

Validation respondents noted how inaccuracies and loss of detail were present due to the relative coarseness of the 1 km spatial resolution in comparison to finer grained local reference data. Validators for Turin and Los Angeles specifically noted this limitation in relation to the POPD layer. However, the POPD layer for Mexico City was noted as relatively accurate compared to census tract level population data considering the difference in spatial resolution. In relation to the IMR input, respondents for Maiduguri noted how "there are a few subtle variances across the city that are not captured … perhaps, due to a lack of data at the census track level".

The Mexico City validators noted that some areas of the NDBI layer did not accurately reflect urban built up areas, specifically sparsely vegetated mountain and hill areas on the outskirts of the urban centre. Validators for Changsha suggested that water bodies could be considered in the GUHVI calculation, as this may reveal differences in heat vulnerability between cities and areas with and without this land cover typology.

From the second round of validation feedback on updates to the methodology, respondents for eight out of nine cities agreed that the calculated hottest period accurately aligned that of the 2023 target year. According to the Los Angeles validator, 1st July to 1st November would have slightly more accurately reflected the specific target year of 2023, compared to the previous five-year average hottest period identified as 1st June to 1st October. All validators endorsed the methodological update to only reduce weighting of pixels overlapping ocean, and this change resulted in higher alignment with local observations.

4. Discussion

4.1. Heat vulnerability insights

Urban heat is an increasingly pressing public health problem globally, significantly increasing mortality and morbidity during heatwaves (Zhao et al., 2021). We developed and tested the international application and validity of a GUHVI for systematic measurement of the spatial distribution of heat vulnerability. We found that the GUHVI was applicable and able to be consistently assessed for diverse cities using global open data. Normalized mean values of heat exposure, heat sensitivity, adaptive capability, and resultant heat vulnerability provided comparable results that could be used to gauge differences between cities across different geographical and climatic regions. There appeared to be a positive correlation between income group and adaptive capability across the included cities. Yet, stronger adaptive capability did not imply reduced heat sensitivity or overall vulnerability. Combining the three components of heat exposure, heat sensitivity and adaptive capability provided an overall picture of heat vulnerability. Our open data methodology was able to show distribution patterns of heat vulnerability spatially and in relation to population distribution. This unveiled within city differences crucial to understanding specific nuances of heat vulnerability in each city, to help target local adaptation efforts. For each city, the maximum heat vulnerability class contained the highest percentage of the overall population. This appears to indicate that the population tends to be more concentrated in areas that are most vulnerable to heat, which may be partly because the most dense, built-up areas are most sensitive to heat (Guo et al., 2025). Population density itself was an input into the GUHVI, so the population living in highly vulnerable areas may have been overestimated. Yet, as one of ten equally weighted inputs, its influence is not significant.

4.2. Australian city comparisons

For five of the eight Australia cities, there was good agreement between the GUHVI results and the iHVI across the majority of the city, with over 75 % class agreement or near-agreement. Canberra had the lowest levels of exact, or near-agreement compared with the iHVI (63.98 %), whereas Melbourne, Perth and Sydney had the highest levels of reasonable agreement, at over 80 %. The iHVI's methodology of excluding SA1s without residents may have contributed to discrepancies between the indexes, as less overall area was

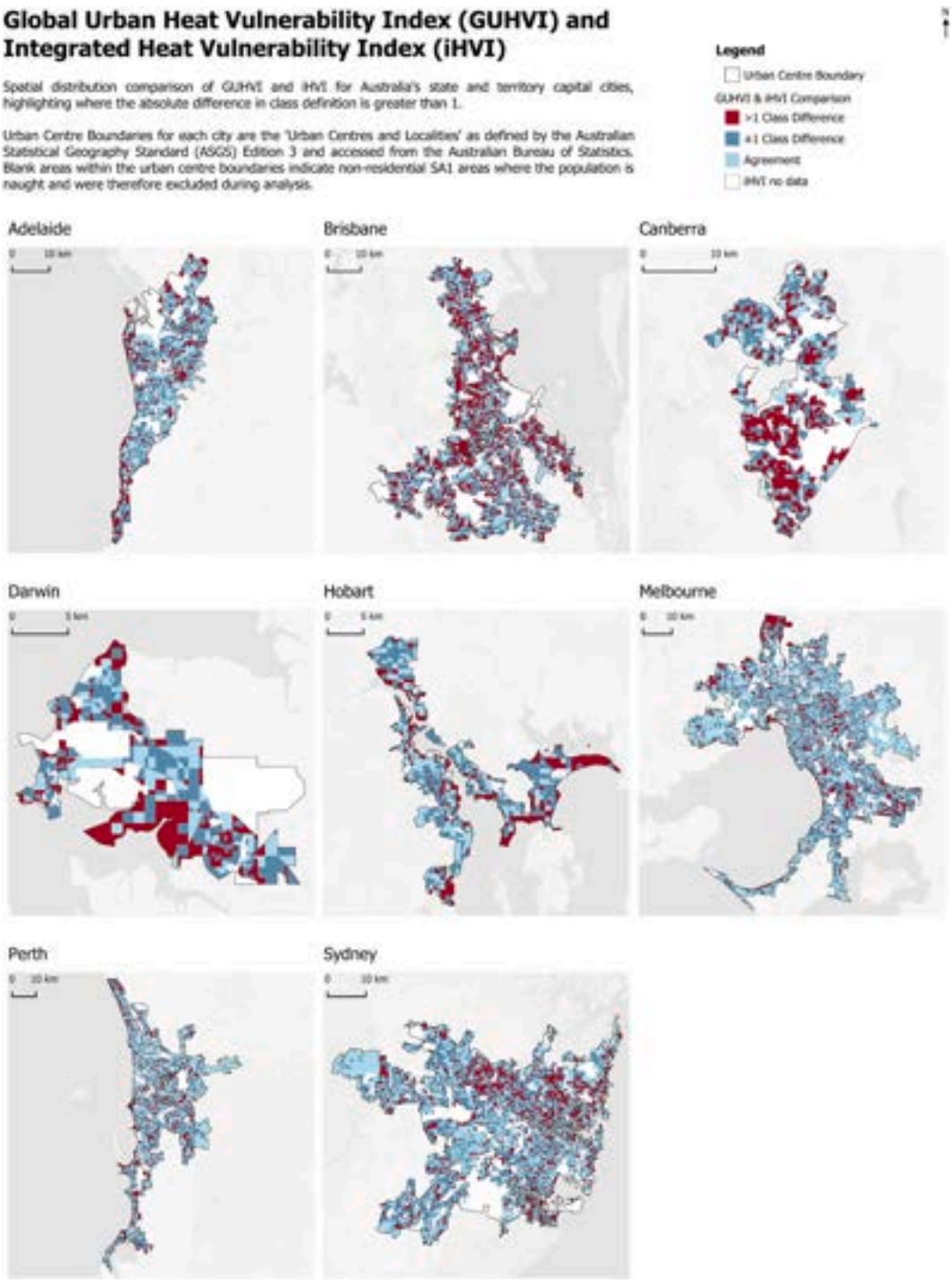

Fig. 6. Areas of heat vulnerability class agreement and disagreement between the GUHVI and iHVI.

considered in the percentile operation for that index, compared to the GUHVI which considered the entire urban centre boundary. In some cases, significant areas were excluded in the iHVI, with Darwin and Canberra having 37.06 % and 30.28 % of the total urban centre excluded, respectively.

The Pearson's correlation coefficients all indicate positive correlation between the GUHVI and iHVI. A pattern emerges based on the urban centre boundary area size. In general, the larger cities of Melbourne, Sydney, Brisbane and Perth had the strongest correlation between the GUHVI and iHVI, with the smaller cities of Darwin and Canberra having the weakest correlation. Hobart is an

exception to this pattern however, perhaps because its percentage of absent iHVI was the smallest of all cities at only 5 %, indicating relatively less impact on the percentile operation. These finding may suggest that the coarseness of the GUHVI's 1 km resolution was more noticeable when overlaid in comparison to the SA1s used in the iHVI in the smaller cities, and therefore resulted in weaker correlation, with the inverse true for the geographically larger cities.

However, this pattern may also be because smaller cities inherently have smaller variability in the inputs used in the two heat indexes, and when combined with relative coarseness of the 1 km resolution of the GUHVI, a strong linear relationship becomes more difficult to statistically detect (Pogson and Smith, 2015). The 1 km resolution of the GUHVI was the finest possible based on the resolutions of the data sources used (see section 2.1), however, a finer resolution index may be able to more accurately reveal statistical correlation in geographically smaller cities.

These statistical validation findings indicate reasonable consistency between our global open data approach and the Australian-specific data, however, differences in native data format may have contributed to the levels of disagreement observed between the two heat vulnerability indexes. Inherent spatial inconsistency is seen between the iHVI's census-unit based approach and the GUHVI's uniform raster grid-based approach. Designed for application in Australia, the iHVI makes use of fine-grained census-tract level data at the nationally consistent SA1 level. This ensures high applicability for Australian local governments, practitioners, or other policy-outcome minded users of this tool. However, boundaries informed by political jurisdiction have inconsistent form, scale and area. For example, highly populated SA1s in inner-city regions are typically much smaller in area than regional SA1s as these are population-based catchments. Despite the relative coarseness of the GUHVI's 1 km resolution, a raster-grid based approach presents advantages over a census-unit based approach that are better aligned with the international application of the GUHVI. The raster grid presents information unrestricted by artificial municipality boundaries that can neither contain nor exacerbate heat, and its uniformity enables comparability across different cities globally. Our GUHVI findings contribute to the growing body of literature that highlight the merits of a grid-based approach in urban heat vulnerability assessments (Sun et al., 2022b; Zhang et al., 2018).

Except for both indexes using LST as the sole input for the heat exposure index, several differences in the selection of other data inputs may have also contributed to the levels of disagreement observed. The iHVI placed heavy importance on population demographics with six of its nine total inputs related to this. As an Australian-specific heat vulnerability index, the iHVI was able to make use of Australian census data to capture finer details of population demographics and include these more nuanced details in its heat vulnerability assessment framework. Contrastingly, the GUHVI had five of its ten total inputs related to population demographics (POPD, POPV, CDR, SHDI, IMR). The remaining half of the GUHVI inputs described natural and built environment characteristics and extended on the iHVI methodology by including LSA and LCZ. This balance between input categories in the GUHVI more evenly describe aspects known to influence heat vulnerability (Kim and Kim, 2024) and serve as a default framework for global application.

4.3. Validated indicators for cities internationally

Our validation approach with local collaborators endorsed the GUHVI's ability to identify spatial inequities in heat vulnerability with sufficient accuracy, based on their lived experience and knowledge of their city. Our methodology using global open data is applicable for cities internationally, offering a consistent measurement approach. This could reduce barriers to calculating urban heat vulnerability worldwide, especially in cities and regions without high-quality official data sources.

To align with our aims of international application, we used remote sensing data to programmatically identify the hottest period of the year. Rather than determining the hottest period based on data of the target year alone, we used a previous five-year average LST calculation. This more robust methodology results in a solution informed by a larger and richer dataset that negates inherent limitations of satellite imagery due to cloud cover. Five years was determined as a suitable balance between capturing more recent and, therefore, relevant temperature characteristics and cloud computing demands. This methodology was endorsed by collaborators as a suitable default parameter that ensures heat vulnerability calculation aligns with the hottest period of the year, the accuracy of which was confirmed for eight of nine cities. For Los Angeles, the average temperature of the period from 1st June to 1st October was found to be 1.2 °C greater than that of the period 1st July to 1st November, thus indicating a very slight preference to the former data range. The open-source nature of the GUHVI allowed us to build in the capability for users to modify the hottest period of the year to align with the specific target year if desired.

The strength of NDBI is its ability to identify impervious surfaces with minimal vegetation such as concrete or asphalt. However, bare soil and exposed rock have a similar spectral signature to these urban land cover typologies. Therefore, some peri-urban areas in Mexico City returned a high NDBI reading which inaccurately indicated built-up areas. This finding highlights a limitation of the NDBI input, and careful consideration should be applied to cities of typically dry climates such as Mexico City. One approach to avoid this would be to ensure that the urban centre boundary does not contain any expanses of bare soil or exposed rock larger than approximately 1 km^2 if their presence does not accurately represent built-up areas, or alternatively, substitute NDBI with an appropriate local land cover typology dataset. Recent advances in machine learning-based techniques for urban remote sensing may offer viable alternatives to improve accuracy in land cover categorisation for urban heat vulnerability research (Li et al., 2024a).

As noted by collaborators in Changsha, we did not include water bodies as an explicit input in the GUHVI. Our coastal pixel overlap methodology and custom LCZ order, which placed water as the least heat retaining, was the extent of the GUHVI's consideration of water bodies. Evidence suggests that water bodies may be valuable for climate and heat-related health (Hunter et al., 2023; Wang et al., 2022). However, more research is needed to determine the impact of water bodies on heat vulnerability assessments due to their potential impact on nocturnal warming, and their cooling effectiveness being dependent on additional external factors such as wind and humidity, which were not captured in the GUHVI (Gunawardena et al., 2017). These other climatic variables may also be relevant for inclusion in heat vulnerability assessments, however, consistent data sources with global coverage is lacking to confidently include

these highly dynamic variables.

The quality and granularity of worldwide socio-economic data available at the sub-city scale may be a limitation of our approach. Validation comments identified that the ACI index was spatially homogenous compared to the HEI and HSI. While we considered reducing the weighting of this index in the GUHVI calculation, the approach of equally weighted inputs followed approaches used in previous studies (Li et al., 2024b). The Subnational Human Development Index (SHDI), and Infant Mortality Rates (IMR) inputs for the ACI were derived from the Global Gridded Relative Depravation Index (GRDI) (Center for International Earth Science Information Network (CIESIN) Columbia University, 2022). These inputs were chosen as they were the closest approximation of the iHVI data inputs. A search of existing literature found the GRDI to be the most suitable data source for the purposes of this study, and the authors are unaware of any alternative gridded socio-economic data with worldwide coverage and finer spatial resolution than 1 km.

Official government data may be more suitable for cities and regions where high-quality data are available. We encourage users to adapt the GUHVI inputs as required to best represent local conditions. Based on the results of this study, substitution of the CDR, SHDI and IMR with appropriate local data at finer resolutions could further enhance the ability of the ACI to distinguish levels of heat vulnerability within urban centres of any city worldwide.

Our combination of quantitative and qualitative validation presents a holistic assessment of the robustness of the GUHVI. Complementary to our spatial comparison between the iHVI and GUHVI for eight Australian cities, our international collaboration with experts in nine diverse cities provides insights informed by local knowledge. Previous heat vulnerability assessments (Li et al., 2022) have not been validated using both quantitative and qualitative methods, which may miss the complex nature of heat vulnerability in urban contexts and limit effective policy making.

4.4. Recommendations for policy and practice

The GUHVI provides actionable evidence to inform policy and practice. The spatial nature of the outputs show within-city spatial inequities in heat vulnerability at the neighbourhood scale. These insights help with prioritising interventions in areas of greatest need to reduce inequities in the health impacts of heat.

The international comparability of the GUHVI also offers opportunities for informing local policy formulation. Policymakers may use the GUHVI methodology to compare results in cities of similar geographic location, climatic zone or socio-economic status, and investigate the latter's policy precedence and best practices. While the GUHVI may help identify vulnerable populations using a data driven approach, other sources of evidence including local knowledge and community engagement are required to formulate appropriate interventions for specific contexts. As a complement to local evidence, the GUHVI approach can help decision makers be more informed and equipped to fill policy gaps in response to heat-related issues.

The findings for the GUHVI and its sub-indexes could also help decisionmakers to specifically target modifiable risk factors of urban heat vulnerability. For example, Los Angeles' relatively high mean HEI identified by our methods suggests that land surface temperature should be reduced to lower overall heat vulnerability. Nature-based solutions and green infrastructure including urban trees and green roofs are an effective way for cities to reduce heat exposure (Esperon-Rodriguez et al., 2025; Guo et al., 2023; Iungman et al., 2023). Heat-exacerbating artificial grey space, such as car parks can be converted into green spaces (Croeser et al., 2022). Other approaches to mitigating heat can include using roofing and pavement materials that reduce heat absorption and increase reflectance (Liu et al., 2024; Ziaeemehr et al., 2023), improving the thermal efficiency of homes, and other shading and cooling mechanisms for public spaces, including cool routes for active travel and cooling centres in which to take refuge from the heat. Heat-sensitive urban planning and design interventions and public awareness campaigns about staying safe in heatwaves can also target specific vulnerable groups to reduce inequities in adaptive capability (O'Neill et al., 2009).

4.5. Future research

Differing climatic, societal and cultural settings between cities and countries infer that pre-identified vulnerability indicators should not be considered as universally applicable (Hondula et al., 2015). The GUHVI presents an internationally validated set of default parameters in terms of hottest third of the year and open data sources. However, users are encouraged to modify parameters (e.g. using data across multi-year time periods), as they see fit to better inform their local context for better outcomes. Integration of the GUHVI into the open-source GHSCI software as part of the next steps in this research project will provide opportunities to validate the indicators for a wider range of cities and explore ways in which users interact with the software and apply the indicator outputs in research and practice.

5. Conclusion

Built entirely from open data and configurable to use custom data where available and preferred, the GUHVI generates insights into the spatial distribution of heat vulnerability across cities worldwide, highlighting priority areas requiring intervention. We adapted an Australian heat vulnerability index for global application by substituting inputs with open data to enable consistent measurement and generate comparable outputs. With a focus on worldwide urban measurement, the GUHVI was tested and validated for diverse cities, drawing on local collaborator knowledge and spatial comparisons. The resulting internationally applicable index facilitates more accurate and consistent benchmarking, comparative analyses, and actionable neighbourhood-level insights for cities worldwide. This advances the capacity to monitor and reduce heat vulnerability and promote climate resilience in planning strategies. The GUHVI enhances equity in access to evidence-generating tools that can directly inform research and efforts to reduce heat vulnerability and

adapt urban environments to mitigate the adverse effects of heat on human health.

CRediT authorship contribution statement

Ryan Turner: Writing – review & editing, Writing – original draft, Visualization, Software, Methodology, Formal analysis, Data curation, Conceptualization. **Carl Higgs:** Writing – review & editing, Writing – original draft, Methodology, Conceptualization. **Chayn Sun:** Writing – review & editing, Writing – original draft, Methodology, Conceptualization. **Eugen Resendiz:** Writing – review & editing, Validation. **Ke Peng:** Writing – review & editing, Validation. **Xiaoyu Cheng:** Writing – review & editing, Validation. **Ruth Hunter:** Writing – review & editing, Validation. **Geoff Boeing:** Writing – review & editing, Validation. **Daria Pugacheva:** Writing – review & editing, Validation. **Ruoyu Chen:** Writing – review & editing, Validation. **Deepti Adlakha:** Writing – review & editing, Validation. **Vedankur Kedar:** Writing – review & editing, Validation. **Giovani Longo Rosa:** Writing – review & editing, Validation. **Adewale Oyeyemi:** Writing – review & editing, Validation. **Rossano Schifanella:** Writing – review & editing, Validation. **Pau Serra del Pozo:** Writing – review & editing, Validation. **Gonzalo Peraza-Mues:** Validation. **Joanna Valson:** Validation. **Ester Cerin:** Writing – review & editing. **Anna Puig-Ribera:** Writing – review & editing. **Erica Hinckson:** Writing – review & editing. **Melanie Lowe:** Writing – review & editing, Writing – original draft, Project administration, Methodology, Funding acquisition, Conceptualization.

Declaration of competing interest

Melanie Lowe reports financial support was provided by AXA Research Fund. Eugen Resendiz reports financial support was provided by People, Health & Place lab (PI: Deborah Salvo) at the Department of Kinesiology and Health Education of the University of Texas at Austin and Tecnologico de Monterrey under the Challenge-Based Research Funding Ruta Azul Program 2023 (CCM-TM-12-166). Ruth Hunter and Joanna Valson report financial support was provided by National Institute of Aging (R01AG030153). Ruth Hunter reports financial support was provided by Economic and Social Research Council and Innovate UK under the Healthy Ageing Challenge Social, Behavioural and Design Research Programme Fund [ES/V016075/1]. Adewale Oyeyemi reports financial support was provided by National Heart, Lung, And Blood Institute of the National Institutes of Health (R21HL175536). Melanie Lowe, Carl Higgs, Eugen Resendiz, Geoff Boeing, Deepti Adlakha, Ester Cerin, and Erica Hinckson report a relationship with The Global Observatory of Healthy and Sustainable Cities that includes executive committee membership. The remaining authors declare that they have no known competing financial interests or personal relationships that could have appeared to influence the work reported in this paper.

Data availability

All research data, code and validation material are available at https://doi.org/10.25439/rmt.28581179

References

Alonso, L., Renard, F., 2020. A comparative study of the physiological and socio-economic vulnerabilities to heat waves of the population of the Metropolis of Lyon (France) in a climate change context. Int. J. Environ. Res. Public Health 17 (3), 1004. https://doi.org/10.3390/ijerph17031004.

Amoatey, P., Trancoso, R., Xu, Z., Darssan, D., Osborne, N.J., Phung, D., 2025. Evaluating the association between heatwave vulnerability index and related deaths in Australia. Environ. Impact Assess. Rev. 112, 107812. https://doi.org/10.1016/j.eiar.2025.107812.

Aram, F., Higueras García, E., Solgi, E., Mansournia, S., 2019. Urban green space cooling effect in cities. Heliyon 5 (4), e01339. https://doi.org/10.1016/j.heliyon.2019.e01339.

Auffhammer, M., Baylis, P., Hausman, C.H., 2017. Climate change is projected to have severe impacts on the frequency and intensity of peak electricity demand across the United States. Proc. Natl. Acad. Sci. USA 114 (8), 1886–1891. https://doi.org/10.1073/pnas.1613193114.

Australian Bureau of Statistics, 2021. Statistical Area Level 1. ABS. https://www.abs.gov.au/statistics/standards/australian-statistical-geography-standard-asgs-edition-3/jul2021-jun2026/main-structure-and-greater-capital-city-statistical-areas/statistical-area-level-1.

Australian Bureau of Statistics, 2022. Urban Centres and Localities. ABS. https://www.abs.gov.au/statistics/standards/australian-statistical-geography-standard-asgs-edition-3/jul2021-jun2026/significant-urban-areas-urban-centres-and-localities-section-state/urban-centres-and-localities.

Bai, Y., Liao, S., Sun, J., 2011. Scale effect and methods for accuracy evaluation of attribute information loss in rasterization. J. Geogr. Sci. 21 (6), 1089–1100. https://doi.org/10.1007/s11442-011-0902-1.

Beck, H.E., Zimmermann, N.E., McVicar, T.R., Vergopolan, N., Berg, A., Wood, E.F., 2018. Present and future Köppen-Geiger climate classification maps at 1-km resolution. Sci. Data 5 (1), 180214. https://doi.org/10.1038/sdata.2018.214.

Bosomworth, K., Trundle, A., McEvoy, D., 2013. Responding to the Urban Heat Island: A Policy and Institutional Analysis. Victorian Centre for Climate Change Adaptation Research Melbourne. https://doi.org/10.25439/rmt.27349284.

Cai, Z., Tang, Y., Chen, K., Han, G., 2019. Assessing the heat vulnerability of different local climate zones in the old areas of a Chinese megacity. Sustainability 11 (7), 2032. https://doi.org/10.3390/su11072032.

Cao, Q., Yu, D., Georgescu, M., Wu, J., Wang, W., 2018. Impacts of future urban expansion on summer climate and heat-related human health in eastern China. Environ. Int. 112, 134–146. https://doi.org/10.1016/j.envint.2017.12.027.

Center for International Earth Science Information Network (CIESIN) Columbia University, 2022. Global Gridded Relative Deprivation Index (GRDI), Version 1. NASA Socioeconomic Data and Applications Center (SEDAC). https://doi.org/10.7927/3xxe-ap97.

Chambers, J., 2020. Global and cross-country analysis of exposure of vulnerable populations to heatwaves from 1980 to 2018. Clim. Chang. 163 (1), 539–558. https://doi.org/10.1007/s10584-020-02884-2.

Cheng, W., Li, D., Liu, Z., Brown, R.D., 2021. Approaches for identifying heat-vulnerable populations and locations: A systematic review. Sci. Total Environ. 799, 149417. https://doi.org/10.1016/j.scitotenv.2021.149417.

Congalton, R., 1997. Exploring and evaluating the consequences of vector-to-raster and raster-to-vector conversion. Photogramm. Eng. Remote. Sens. 63, 425–434. https://scholars.unh.edu/faculty_pubs/1359/.

Coutts, A., Beringer, J., Tapper, N., 2010. Changing Urban climate and CO2 emissions: implications for the development of policies for sustainable cities. Urban Policy Res. 28 (1), 27–47. https://doi.org/10.1080/08111140903437716.
Croeser, T., Garrard, G.E., Visintin, C., Kirk, H., Ossola, A., Furlong, C., Clements, R., Butt, A., Taylor, E., Bekessy, S.A., 2022. Finding space for nature in cities: the considerable potential of redundant car parking. npj Urban Sustain. 2 (1), 27. https://doi.org/10.1038/s42949-022-00073-x.
Cruz, M., Ahmed, S.A., 2018. On the impact of demographic change on economic growth and poverty. World Dev. 105, 95–106. https://doi.org/10.1016/j.worlddev.2017.12.018.
Demuzere, M., Kittner, J., Martilli, A., Mills, G., Moede, C., Stewart, I.D., van Vliet, J., Bechtel, B., 2022. A global map of local climate zones to support earth system modelling and urban-scale environmental science. Earth Syst. Sci. Data 14 (8), 3835–3873. https://doi.org/10.5194/essd-14-3835-2022.
Dimitrova, A., Dimitrova, A., Mengel, M., Gasparrini, A., Lotze-Campen, H., Gabrysch, S., 2024. Temperature-related neonatal deaths attributable to climate change in 29 low- and middle-income countries. Nat. Commun. 15 (1), 5504. https://doi.org/10.1038/s41467-024-49890-x.
Earth Resources Observation and Science (EROS) Center, 2020a. Landsat 8–9 Operational Land Imager / Thermal Infrared Sensor Level-1, Collection 2 [Dataset]. U.S. Geological Survey. https://doi.org/10.5066/P975CC9B.
Earth Resources Observation and Science (EROS) Center, 2020b. Landsat 8–9 Operational Land Imager / Thermal Infrared Sensor Level-2, Collection 2 [Dataset]. U.S. Geological Survey. https://doi.org/10.5066/P9OGBGM6.
Eifling, K.P., Gaudio, F.G., Dumke, C., Lipman, G.S., Otten, E.M., Martin, A.D., Grissom, C.K., 2024. Wilderness medical society clinical practice guidelines for the prevention and treatment of heat illness: 2024 update. Wilderness Environ. Med. 35 (1_suppl), 112S–127S. https://doi.org/10.1177/10806032241227924.
Elizabeth Loughnan, M., J. Tapper, N., Phan, T., A. McInnes, J., 2014. Can a spatial index of heat-related vulnerability predict emergency service demand in Australian capital cities? Int. J. Emerg. Serv. 3 (1), 6–33. https://doi.org/10.1108/IJES-10-2012-0044.
Esperon-Rodriguez, M., Gallagher, R.V., Lenoir, J., Barradas, V.L., Beaumont, L.J., Calfapietra, C., Cariñanos, P., Livesley, S.J., Iungma, T., Manoli, G., Marchin, R.M., McPhearson, T., Messier, C., Nieuwenhuijsen, M., Power, S.A., Rymer, P.D., Tjoelker, M.G., 2025. Urban heat in global cities and the role of nature-based solutions in mitigating future climate risks. Environ. Res. Clim. 4 (2), 023001. https://doi.org/10.1088/2752-5295/adcb61.
Estoque, R.C., Ooba, M., Seposo, X.T., Togawa, T., Hijioka, Y., Takahashi, K., Nakamura, S., 2020. Heat health risk assessment in Philippine cities using remotely sensed data and social-ecological indicators. Nat. Commun. 11 (1), 1581. https://doi.org/10.1038/s41467-020-15218-8.
European Space Agency, 2021. Copernicus Sentinel-2 (Processed by ESA), 2021, MSI Level-2A BOA Reflectance Product Collection 1 [Dataset]. https://doi.org/10.5270/S2_-znk9xsj.
Fan, J.-L., Zeng, B., Hu, J.-W., Zhang, X., Wang, H., 2020. The impact of climate change on residential energy consumption in urban and rural divided southern and northern China. Environ. Geochem. Health 42 (3), 969–985. https://doi.org/10.1007/s10653-019-00430-3.
Florczyk, A., Melchiorri, M., Corban, C., Schiavina, M., Maffenini, L., Pesaresi, M., Politis, P., Sabo, F., Carneiro Freire, S., Ehrlich, D., Kemper, T., Tommasi, P., Airaghi, D., Zanchetta, L., 2019. Description of the GHS Urban Centre Database 2015. Publications Office of the European Union, Luxembourg. https://doi.org/10.2760/037310.
Gauer, R., Meyers, B.K., 2019. Heat-related illnesses. Am. Fam. Physician 99 (8), 482–489.
Global Healthy and Sustainable City-Indicators Collaboration, 2022. Global Observatory of Healthy and Sustainable Cities. https://www.healthysustainablecities.org/.
Gonzalez-Trevizo, M.E., Martinez-Torres, K.E., Armendariz-Lopez, J.F., Santamouris, M., Bojorquez-Morales, G., Luna-Leon, A., 2021. Research trends on environmental, energy and vulnerability impacts of Urban Heat Islands: an overview. Energ. Buildings 246, 111051. https://doi.org/10.1016/j.enbuild.2021.111051.
Guerreiro, S., Dawson, R., Kilsby, C., Lewis, E., Ford, A., 2018. Future heat-waves, droughts and floods in 571 European cities. Environ. Res. Lett. 13, 034009. https://doi.org/10.1088/1748-9326/aaaad3.
Gunawardena, K.R., Wells, M.J., Kershaw, T., 2017. Utilising green and bluespace to mitigate urban heat island intensity. Sci. Total Environ. 584-585, 1040–1055. https://doi.org/10.1016/j.scitotenv.2017.01.158.
Guo, A., He, T., Yue, W., Xiao, W., Yang, J., Zhang, M., Li, M., 2023. Contribution of urban trees in reducing land surface temperature: evidence from China's major cities. Int. J. Appl. Earth Obs. Geoinf. 125, 103570. https://doi.org/10.1016/j.jag.2023.103570.
Guo, F., Fan, G., Zhao, J., Zhang, H., Dong, J., Ma, H., Li, N., 2025. Urban heat health risk inequality and its drivers based on local climate zones: a case study of Qingdao, China. Build. Environ. 275, 112827. https://doi.org/10.1016/j.buildenv.2025.112827.
Harlan, S.L., Chowell, G., Yang, S., Petitti, D.B., Morales Butler, E.J., Ruddell, B.L., Ruddell, D.M., 2014. Heat-related deaths in hot cities: estimates of human tolerance to high temperature thresholds. Int. J. Environ. Res. Public Health 11 (3), 3304–3326. https://doi.org/10.3390/ijerph110303304.
Hess, J.J., Errett, N.A., McGregor, G., Busch Isaksen, T., Wettstein, Z.S., Wheat, S.K., Ebi, K.L., 2023. Public health preparedness for extreme heat events. Annu. Rev. Public Health 44, 301–321. https://doi.org/10.1146/annurev-publhealth-071421-025508.
Higgs, C., Lowe, M., Giles-Corti, B., Boeing, G., Delclòs-Alió, X., Puig-Ribera, A., Adlakha, D., Liu, S., Borello Vargas, J.C., Castillo-Riquelme, M., Jafari, A., Molina-García, J., Heikinheimo, V., Queralt, A., Cerin, E., Resendiz, E., Singh, D., Rodriguez, S., Suel, E., Alderton, A., 2024. Global healthy and sustainable city indicators: collaborative development of an open science toolkit for calculating and reporting on urban indicators internationally. Environ. Plan. B Urban Anal. City Sci. 52 (5), 1252–1270. https://doi.org/10.1177/23998083241292102.
Hondula, D.M., Davis, R.E., Saha, M.V., Wegner, C.R., Veazey, L.M., 2015. Geographic dimensions of heat-related mortality in seven U.S. cities. Environ. Res. 138, 439–452. https://doi.org/10.1016/j.envres.2015.02.033.
Hunter, R.F., Nieuwenhuijsen, M., Fabian, C., Murphy, N., O'Hara, K., Rappe, E., Sallis, J.F., Lambert, E.V., Duenas, O.L.S., Sugiyama, T., Kahlmeier, S., 2023. Advancing urban green and blue space contributions to public health. Lancet Public Health 8 (9), e735–e742. https://doi.org/10.1016/S2468-2667(23)00156-1.
IPCC, 2022. Climate Change 2022 – Impacts, Adaptation and Vulnerability: Working Group II Contribution to the Sixth Assessment Report of the Intergovernmental Panel on Climate Change. Cambridge University Press. https://doi.org/10.1017/9781009325844.
Iungman, T., Cirach, M., Marando, F., Pereira Barboza, E., Khomenko, S., Masselot, P., Quijal-Zamorano, M., Mueller, N., Gasparrini, A., Urquiza, J., Heris, M., Thondoo, M., Nieuwenhuijsen, M., 2023. Cooling cities through urban green infrastructure: a health impact assessment of European cities. Lancet 401 (10376), 577–589. https://doi.org/10.1016/S0140-6736(22)02585-5.
Jandaghian, Z., Akbari, H., 2021. Increasing urban albedo to reduce heat-related mortality in Toronto and Montreal, Canada. Energ. Buildings 237, 110697. https://doi.org/10.1016/j.enbuild.2020.110697.
Kant, Y., Shaik, D.S., Mitra, D., Chandola, H.C., Babu, S.S., Chauhan, P., 2020. Black carbon aerosol quantification over north-West Himalayas: seasonal heterogeneity, source apportionment and radiative forcing. Environ. Pollut. 257, 113446. https://doi.org/10.1016/j.envpol.2019.113446.
Karanja, J., Kiage, L., 2021. Perspectives on spatial representation of urban heat vulnerability. Sci. Total Environ. 774, 145634. https://doi.org/10.1016/j.scitotenv.2021.145634.
Kenny, G.P., Yardley, J., Brown, C., Sigal, R.J., Jay, O., 2010. Heat stress in older individuals and patients with common chronic diseases. Cmaj 182 (10), 1053–1060. https://doi.org/10.1503/cmaj.081050.
Kim, Y., Kim, Y., 2024. An analytical framework for assessing heat vulnerability in urban thermal environmental planning. Urban Clim. 58, 102145. https://doi.org/10.1016/j.uclim.2024.102145.
Li, F., Yigitcanlar, T., Nepal, M., Thanh, K.N., Dur, F., 2022. Understanding urban heat vulnerability assessment methods: a PRISMA review. Energies 15 (19), 6998. https://doi.org/10.3390/en15196998.
Li, S., Yan, Q., Liu, Z., Wang, X., Yu, F., Teng, D., Sun, Y., Lu, D., Zhang, J., Gao, T., Zhu, J., 2023. Seasonality of albedo and fraction of absorbed photosynthetically active radiation in the temperate secondary forest ecosystem: a comprehensive observation using Qingyuan Ker towers. Agric. For. Meteorol. 333, 109418. https://doi.org/10.1016/j.agrformet.2023.109418.
Li, F., Yigitcanlar, T., Li, W., Nepal, M., Nguyen, K., Dur, F., 2024a. Understanding urban heat vulnerability: scientometric analysis of five decades of research. Urban Clim. 56, 102035. https://doi.org/10.1016/j.uclim.2024.102035.

Li, F., Yigitcanlar, T., Nepal, M., Nguyen, K., Dur, F., Li, W., 2024b. Assessing heat vulnerability and multidimensional inequity: lessons from indexing the performance of Australian capital cities. Sustain. Cities Soc. 115, 105875. https://doi.org/10.1016/j.scs.2024.105875.
Liang, S., 2001. Narrowband to broadband conversions of land surface albedo I: algorithms. Remote Sens. Environ. 76 (2), 213–238. https://doi.org/10.1016/S0034-4257(00)00205-4.
Liu, X., Yue, W., Yang, X., Hu, K., Zhang, W., Huang, M., 2020. Mapping Urban heat vulnerability of extreme heat in Hangzhou via comparing two approaches. Complexity 2020 (1), 9717658. https://doi.org/10.1155/2020/9717658.
Liu, Y., Chu, C., Zhang, R., Chen, S., Xu, C., Zhao, D., Meng, C., Ju, M., Cao, Z., 2024. Impacts of high-albedo urban surfaces on outdoor thermal environment across morphological contexts: a case of Tianjin, China. Sustain. Cities Soc. 100, 105038. https://doi.org/10.1016/j.scs.2023.105038.
Lu, L., Fu, P., Dewan, A., Li, Q., 2023. Contrasting determinants of land surface temperature in three megacities: implications to cool tropical metropolitan regions. Sustain. Cities Soc. 92, 104505. https://doi.org/10.1016/j.scs.2023.104505.
Luo, Y., Yang, J., Shi, Q., Xu, Y., Menenti, M., Wong, M.S., 2023. Seasonal cooling effect of vegetation and albedo applied to the LCZ classification of three Chinese megacities. Remote Sens. 15 (23), 5478. https://doi.org/10.3390/rs15235478.
Martín, Y., Paneque, P., 2022. Moving from adaptation capacities to implementing adaptation to extreme heat events in urban areas of the European Union: introducing the U-ADAPT! research approach. J. Environ. Manag. 310, 114773. https://doi.org/10.1016/j.jenvman.2022.114773.
Münzel, T., Hahad, O., Sørensen, M., Lelieveld, J., Duerr, G.D., Nieuwenhuijsen, M., Daiber, A., 2022. Environmental risk factors and cardiovascular diseases: a comprehensive expert review. Cardiovasc. Res. 118 (14), 2880–2902. https://doi.org/10.1093/cvr/cvab316.
O'Neill, M.S., Carter, R., Kish, J.K., Gronlund, C.J., White-Newsome, J.L., Manarolla, X., Zanobetti, A., Schwartz, J.D., 2009. Preventing heat-related morbidity and mortality: new approaches in a changing climate. Maturitas 64 (2), 98–103. https://doi.org/10.1016/j.maturitas.2009.08.005.
OpenStreetMap Contributors, 2024. OpenStreetMap. OpenStreetMap Foundation. www.openstreetmap.org.
Parsons, K., 2009. Maintaining health, comfort and productivity in heat waves. Glob. Health Action 2 (1), 2057. https://doi.org/10.3402/gha.v2i0.2057.
Pogson, M., Smith, P., 2015. Effect of spatial data resolution on uncertainty. Environ. Model Softw. 63, 87–96. https://doi.org/10.1016/j.envsoft.2014.09.021.
QGIS Development Team, 2024. QGIS Geographic Information System (QGIS Version 3.34). Open Source Geospatial Foundation Project. https://qgis.org/.
Qian, Y., Liu, T., 2025. Heat vulnerability assessment: a systematic review of critical metrics. Hygiene Environ. Health Adv. 15, 100138. https://doi.org/10.1016/j.heha.2025.100138.
Rahmani, N., Sharifi, A., 2025. Urban heat dynamics in local climate zones (LCZs): a systematic review. Build. Environ. 267, 112225. https://doi.org/10.1016/j.buildenv.2024.112225.
Reid, C.E., O'Neill, M.S., Gronlund, C.J., Brines, S.J., Brown, D.G., Diez-Roux, A.V., Schwartz, J., 2009. Mapping community determinants of heat vulnerability. Environ. Health Perspect. 117 (11), 1730–1736. https://doi.org/10.1289/ehp.0900683.
Reid, C.E., Mann, J.K., Alfasso, R., English, P.B., King, G.C., Lincoln, R.A., Margolis, H.G., Rubado, D.J., Sabato, J.E., West, N.L., Woods, B., Navarro, K.M., Balmes, J. R., 2012. Evaluation of a heat vulnerability index on abnormally hot days: an environmental public health tracking study. Environ. Health Perspect. 120 (5), 715–720. https://doi.org/10.1289/ehp.1103766.
Reidpath, D.D., Allotey, P., 2003. Infant mortality rate as an indicator of population health. J. Epidemiol. Community Health 57 (5), 344–346. https://doi.org/10.1136/jech.57.5.344.
Saguansap, P., Saguansap, V., Mruksirisuk, P., Thanvisitthpon, N.T., 2024. Assessment of urban heat island vulnerability using sustainability-focused framework: a case study of Thailand's Bangkok Metropolis. Curr. Res. Environ. Sustain. 8, 100262. https://doi.org/10.1016/j.crsust.2024.100262.
Sailor, D.J., Georgescu, M., Milne, J.M., Hart, M.A., 2015. Development of a national anthropogenic heating database with an extrapolation for international cities. Atmos. Environ. 118, 7–18. https://doi.org/10.1016/j.atmosenv.2015.07.016.
Salamanca, F., Georgescu, M., Mahalov, A., Moustaoui, M., Wang, M., 2014. Anthropogenic heating of the urban environment due to air conditioning. J. Geophys. Res. Atmos. 119 (10), 5949–5965. https://doi.org/10.1002/2013JD021225.
Santamouris, M., Cartalis, C., Synnefa, A., Kolokotsa, D., 2015. On the impact of urban heat island and global warming on the power demand and electricity consumption of buildings—A review. Energ. Buildings 98, 119–124. https://doi.org/10.1016/j.enbuild.2014.09.052.
Schell, C.O., Reilly, M., Rosling, H., Peterson, S., EkstrÖM, A.M., 2007. Socioeconomic determinants of infant mortality: a worldwide study of 152 low-, middle-, and high-income countries. Scand. J. Public Health 35 (3), 288–297. https://doi.org/10.1080/14034940600979171.
Schiavina, M., Melchiorri, M., Pesaresi, M., Politis, P., Carneiro Freire, S.M., Maffenini, L., Florio, P., Ehrlich, D., Goch, K., Carioli, A., Uhl, J., Tommasi, P., Kemper, T., 2023. GHSL Data Package 2023. Publications Office of the European Union. https://doi.org/10.2760/098587.
Shahfahad, Talukdar, S., Naikoo, M.W., Rihan, M., Mohammad, P., Rahman, A., 2024. Seasonal dynamics of land surface temperature and urban thermal comfort with land use land cover pattern in semi-arid Indian cities: insights for sustainable urban management. Urban Clim. 57, 102105. https://doi.org/10.1016/j.uclim.2024.102105.
Smits, J., Permanyer, I., 2019. The subnational human development database. Sci. Data 6 (1), 190038. https://doi.org/10.1038/sdata.2019.38.
Stewart, I.D., Oke, T.R., 2012. Local climate zones for urban temperature studies. Bull. Am. Meteorol. Soc. 93 (12), 1879–1900. https://doi.org/10.1175/BAMS-D-11-00019.1.
Sun, C., Hurley, J., Amati, M., Arundel, J., Saunders, A., Boruff, B., Caccetta, P., 2019. Urban Vegetation, Urban Heat Islands and Heat Vulnerability Assessment in Melbourne, 2018. https://researchrepository.rmit.edu.au/esploro/outputs/9921888097701341.
Sun, Q.C., Macleod, T., Both, A., Hurley, J., Butt, A., Amati, M., 2021. A human-centred assessment framework to prioritise heat mitigation efforts for active travel at city scale. Sci. Total Environ. 763, 143033. https://doi.org/10.1016/j.scitotenv.2020.143033.
Sun, C., Das, S., Wang, K., Tao, Y., Amati, M., Hurley, J., Choy, S., Duckham, M., 2022a. iHVI: An open-source toolkit for constructing integrated heat vulnerability index in Australia. Int. Arch. Photogramm. Remote. Sens. Spat. Inf. Sci. 175–182. https://doi.org/10.5194/isprs-archives-XLVIII-4-W5-2022-175-2022. XLVIII-4/W5-2022.
Sun, Y., Li, Y., Ma, R., Gao, C., Wu, Y., 2022b. Mapping urban socio-economic vulnerability related to heat risk: a grid-based assessment framework by combing the geospatial big data. Urban Clim. 43, 101169. https://doi.org/10.1016/j.uclim.2022.101169.
Sun, Y., Zhu, S., Wang, D., Duan, J., Lu, H., Yin, H., Tan, C., Zhang, L., Zhao, M., Cai, W., Wang, Y., Hu, Y., Tao, S., Guan, D., 2024. Global supply chains amplify economic costs of future extreme heat risk. Nature 627 (8005), 797–804. https://doi.org/10.1038/s41586-024-07147-z.
Tatem, A.J., 2017. WorldPop, open data for spatial demography. Sci. Data 4 (1), 170004. https://doi.org/10.1038/sdata.2017.4.
The World Bank, 2024. World Bank Country and Lending Groups. https://datahelpdesk.worldbank.org/knowledgebase/articles/906519-world-bank-country-and-lending-groups.
Tong, S., Prior, J., McGregor, G., Shi, X., Kinney, P., 2021. Urban heat: an increasing threat to global health. BMJ 375, n2467. https://doi.org/10.1136/bmj.n2467.
Voelkel, J., Hellman, D., Sakuma, R., Shandas, V., 2018. Assessing vulnerability to urban heat: a study of disproportionate heat exposure and access to refuge by socio-demographic status in Portland, Oregon. Int. J. Environ. Res. Public Health 15 (4), 640. https://doi.org/10.3390/ijerph15040640.
Wan, Z., Hook, S., Hulley, G., 2021. MODIS/Terra Land Surface Temperature/Emissivity Daily L3 Global 1km SIN Grid V061 [Dataset]. NASA EOSDIS Land Processes Distributed Active Archive Center. https://doi.org/10.5067/MODIS/MOD11A1.061.
Wang, K., Sun, Z., Cai, M., Liu, L., Wu, H., Peng, Z., 2022. Impacts of urban blue-green space on residents' health: a bibliometric review. Int. J. Environ. Res. Public Health 19 (23). https://doi.org/10.3390/ijerph192316192.
Wang, S., Sun, Q.C., Huang, X., Tao, Y., Dong, C., Das, S., Liu, Y., 2023. Health-integrated heat risk assessment in Australian cities. Environ. Impact Assess. Rev. 102, 107176. https://doi.org/10.1016/j.eiar.2023.107176.
Wolf, T., McGregor, G., 2013. The development of a heat wave vulnerability index for London, United Kingdom. Weather Climate Extremes 1, 59–68. https://doi.org/10.1016/j.wace.2013.07.004.
Xu, Z., Yi, W., Bach, A., Tong, S., Ebi, K.L., Su, H., Cheng, J., Rutherford, S., 2024. Multimorbidity and emergency hospitalisations during hot weather. eBioMedicine 104, 105148. https://doi.org/10.1016/j.ebiom.2024.105148.

Zhang, W., McManus, P., Duncan, E., 2018. A raster-based subdividing indicator to map urban heat vulnerability: a case study in Sydney, Australia. Int. J. Environ. Res. Public Health 15 (11). https://doi.org/10.3390/ijerph15112516.

Zhao, Q., Guo, Y., Ye, T., Gasparrini, A., Tong, S., Overcenco, A., Urban, A., Schneider, A., Entezari, A., Vicedo-Cabrera, A.M., Zanobetti, A., Analitis, A., Zeka, A., Tobias, A., Nunes, B., Alahmad, B., Armstrong, B., Forsberg, B., Pan, S.-C., Li, S., 2021. Global, regional, and national burden of mortality associated with non-optimal ambient temperatures from 2000 to 2019: a three-stage modelling study. Lancet Planet. Heath 5 (7), e415–e425. https://doi.org/10.1016/S2542-5196(21)00081-4.

Zhou, X., Okaze, T., Ren, C., Cai, M., Ishida, Y., Watanabe, H., Mochida, A., 2020. Evaluation of urban heat islands using local climate zones and the influence of sea-land breeze. Sustain. Cities Soc. 55, 102060. https://doi.org/10.1016/j.scs.2020.102060.

Ziaeemehr, B., Jandaghian, Z., Ge, H., Lacasse, M., Moore, T., 2023. Increasing solar reflectivity of building envelope materials to mitigate urban heat islands: state-of-the-art review. Buildings 13 (11), 2868. https://doi.org/10.3390/buildings13112868.